Article

Cell

Regulated Stochasticity in a Bacterial Signaling Network Permits Tolerance to a Rapid Environmental Change

Graphical Abstract

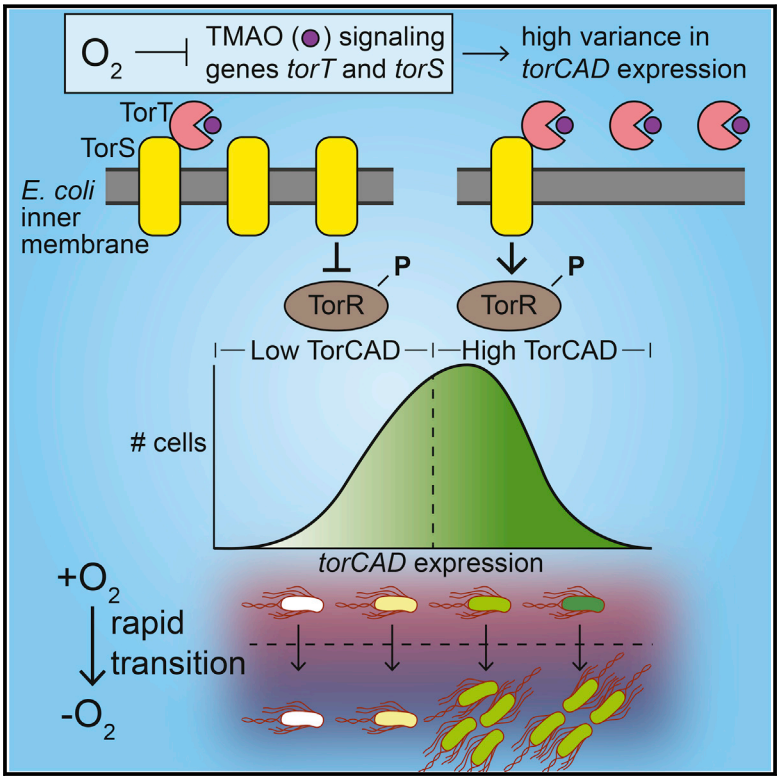

Authors

Jeffrey N. Carey, Erin L. Mettert, Manuela Roggiani, Kevin S. Myers, Patricia J. Kiley, Mark Goulian

Correspondence

goulian@sas.upenn.edu

In Brief

Environmental oxygen regulates the cell-to-cell variability of an *E. coli* signal transduction system that controls anaerobic respiration but leaves the population mean unchanged, thereby revealing a distinct form of bet hedging that provides a fitness advantage when oxygen availability rapidly drops.

Highlights

- Variance in TMAO reductase (*torCAD*) expression allows bet hedging on oxygen loss
- Oxygen-dependent repression of TMAO signaling genes regulates *torCAD* variance
- A point mutation in the repressor binding site derepresses TMAO signaling genes
- In the mutant, *torCAD* is uniformly expressed and bet hedging does not occur

Carey et al., 2018, Cell *173*, 196–207
March 22, 2018
https://doi.org/10.1016/j.cell.2018.02.005

CellPress

Cell

Article

Regulated Stochasticity in a Bacterial Signaling Network Permits Tolerance to a Rapid Environmental Change

Jeffrey N. Carey,[1,2] Erin L. Mettert,[3] Manuela Roggiani,[4] Kevin S. Myers,[3,6] Patricia J. Kiley,[3] and Mark Goulian[4,5,7,*]
[1]Graduate Group in Biochemistry and Molecular Biophysics, Perelman School of Medicine, University of Pennsylvania, Philadelphia, PA 19104, USA
[2]School of Veterinary Medicine, University of Pennsylvania, Philadelphia, PA 19104, USA
[3]Department of Biomolecular Chemistry, School of Medicine and Public Health, University of Wisconsin-Madison, Madison, WI 53706, USA
[4]Department of Biology, University of Pennsylvania, Philadelphia, PA 19104, USA
[5]Department of Physics & Astronomy, University of Pennsylvania, Philadelphia, PA 19104, USA
[6]Present address: Laboratory of Genetics, University of Wisconsin-Madison, Madison, WI 53706, USA
[7]Lead Contact
*Correspondence: goulian@sas.upenn.edu
https://doi.org/10.1016/j.cell.2018.02.005

SUMMARY

Microbial populations can maximize fitness in dynamic environments through bet hedging, a process wherein a subpopulation assumes a phenotype not optimally adapted to the present environment but well adapted to an environment likely to be encountered. Here, we show that oxygen induces fluctuating expression of the trimethylamine oxide (TMAO) respiratory system of *Escherichia coli*, diversifying the cell population and enabling a bet-hedging strategy that permits growth following oxygen loss. This regulation by oxygen affects the variance in gene expression but leaves the mean unchanged. We show that the oxygen-sensitive transcription factor IscR is the key regulator of variability. Oxygen causes IscR to repress expression of a TMAO-responsive signaling system, allowing stochastic effects to have a strong effect on the output of the system and resulting in heterogeneous expression of the TMAO reduction machinery. This work reveals a mechanism through which cells regulate molecular noise to enhance fitness.

INTRODUCTION

Numerous studies have revealed that cell-to-cell variability in gene expression is a common phenomenon in bacteria, and indeed in all domains of life. Depending on context, this heterogeneity in cell behavior can be beneficial or harmful to an organism or population. Accordingly, it has been proposed that diverse gene network architectures have evolved either to generate or limit gene expression variability. In some cases, heterogeneity can benefit a population that experiences unpredictable switching between two or more environments if the different gene expression states confer fitness advantages in different conditions (Kussell and Leibler, 2005; Thattai and van Oudenaarden, 2004; Veening et al., 2008a). This evolutionary strategy, called bet hedging, enables a population to prepare for a potential switch to a new environmental condition by harboring a subpopulation that is pre-adapted to the new environment. Bet hedging has been characterized in a number of microbial systems and shown to play a role in many processes, including pathogenesis (Ackermann et al., 2008; Stewart and Cookson, 2012), antibiotic persistence (Balaban et al., 2004; Maisonneuve and Gerdes, 2014; Verstraeten et al., 2015; Wakamoto et al., 2013), cellular differentiation (Veening et al., 2008b), regulation of metabolism (Hassan et al., 2014; Kotte et al., 2014; Ratcliff and Denison, 2010), induction of stress responses (Sureka et al., 2008), and viral latency (Maslov and Sneppen, 2015; Rouzine et al., 2015). Stochasticity in gene expression is often responsible for the generation of phenotypic diversity in these systems and frequently results in a bimodal distribution of phenotypes (Kotte et al., 2014; Nielsen et al., 2010; Ozbudak et al., 2004; Veening et al., 2008b), although bimodality is not always observed (El Meouche et al., 2016; Levy et al., 2012). Here, we describe a bet hedging mechanism in which an environmental cue induces high variance in gene expression—without changing the mean—and causes individual cells to rapidly traverse a broad distribution of gene expression levels.

Escherichia coli can carry out respiration using trimethylamine oxide (TMAO) instead of oxygen as a terminal electron acceptor through a pathway that requires the gene products of the *torCAD* operon (McCrindle et al., 2005; Méjean et al., 1994; Pommier et al., 1998). Alternative respiratory pathways yield less energy for a cell than aerobic respiration, so most of these systems are repressed when oxygen is present (Unden and Bongaerts, 1997). Surprisingly, TMAO respiration is an exception; in fact, the mean *torCAD* expression across a cell population is independent of oxygen when TMAO is present (Ansaldi et al., 2007; Roggiani and Goulian, 2015). However, *torCAD* transcription is exceptionally noisy in the presence of oxygen but is relatively uniform in its absence, resulting in an oxygen-dependent variance about the mean (Roggiani and Goulian, 2015).

In this work, we show that cell-to-cell variability in aerobic *torCAD* expression enables cells to wager on the possibility of a rapid loss of oxygen by transiently pre-inducing the TMAO respiratory machinery encoded by *torCAD*. We further demonstrate that cells increase variability in *torCAD* transcription in response to oxygen by repressing expression of the TMAO receptor, TorT, and the sensor kinase, TorS, that are part of the signaling system regulating *torCAD*. Importantly, TorS can function as either a kinase or a phosphatase depending on whether or not the protein detects TMAO bound to TorT, making the system sensitive to the relative amounts of TorT and TorS. Stochasticity in the expression of TorT and TorS and/or randomness in their partitioning at cell division generates high variability in downstream expression of *torCAD* without changing the mean. This mechanism for generating regulated phenotypic diversity is a novel strategy for hedging against rapid changes in the environment.

RESULTS

Variability in Aerobic *torCAD* Expression Permits Growth after Oxygen Depletion

Expression of *torCAD* in *E. coli* cells fluctuates rapidly during aerobic growth in the presence of TMAO, resulting in a broad distribution of expression across the population (Movie S1) (see also Roggiani and Goulian, 2015). To assess the plausibility of bet hedging as an explanation for this variability, we tested whether the ability of individual *E. coli* cells to switch to anaerobic TMAO respiration depends on the level of aerobic *torCAD* transcription at the time of oxygen depletion (Figure 1A). Because *E. coli* can grow by fermentation as well as anaerobic respiration, we carried out these experiments in media containing a single, non-fermentable carbon source (glycerol) to ensure that cell growth after oxygen depletion occurred solely by TMAO respiration. We hypothesized that following the transition to low oxygen, cells without a recent history of *torCAD* transcription would suffer a lag in growth, or fail to grow entirely, because they would be unable to produce enough ATP (or other metabolic resources) to synthesize the machinery required for TMAO respiration (TorC and TorA).

To perform these experiments, we developed a method for following single cells through an aerobic-to-anaerobic transition by microscopy (Figure 1B). Cells expressing fluorescent reporters are grown aerobically in liquid culture containing TMAO and a non-fermentable carbon source and then deposited on an agarose pad and sealed between a slide and coverslip. Embedded within the agarose pad are non-fluorescent cells, which scavenge oxygen and rapidly create an anaerobic environment. From measurements using a phosphorescence-based probe (Lebedev et al., 2009), we determined that the oxygen in the agarose pad reaches basal levels in under 5 min after the pads are sealed (data not shown).

We employed this microscopy technique to examine the relationship between *torCAD* expression in single cells at the time of oxygen depletion and the subsequent ability of the cells to grow anaerobically by TMAO respiration. To measure *torCAD* expression, we used a strain that contains a chromosomal copy of the *torCAD* promoter fused to the yellow fluorescent protein (YFP) gene. This P_{torCAD}-*yfp* strain also constitutively expresses mCherry, which allows for the identification of cells of interest regardless of their YFP intensity. We grew this reporter strain aerobically, then deposited a sample on a cell-impregnated agarose pad and captured fluorescence and phase contrast micrographs of randomly selected cells. For each cell, the YFP fluorescence at this starting time point (t = 0) provided a measure of *torCAD* transcription at the time of oxygen depletion. After 5 hr of incubation images were acquired again, and the ratio of microcolony size at 5 hr to the parent cell size at t = 0 was used as a metric of cell growth. A plot of cell growth against YFP fluorescence at the time of transition to anaerobiosis reveals a clear relationship between recent *torCAD* transcription and the ability of cells to thrive following oxygen depletion (Figures 1C and S1A). Interestingly, there appears to be a threshold level of *torCAD* expression below which cells are unable to grow. These results are consistent with bet-hedging behavior, with only the random subpopulation of aerobically growing cells that have synthesized sufficient TorC, TorA, and TorD able to grow after the switch to anaerobiosis. We verified anaerobiosis during these experiments by including a control Δ*torC* strain that will not grow unless oxygen contamination is present (Figures S1B and S1C). We also verified that all cells, regardless of initial YFP fluorescence, are able to grow aerobically (Figure S1D). To further confirm that it is *torCAD* and not other co-regulated genes that allow growth, we conducted a similar experiment to that shown in Figure 1C in which all of the cells in the culture were Δ*torC* and verified that there was no growth after oxygen depletion (Figure S1E).

Expression of *torT* and *torS* Is Elevated in Anaerobic Conditions

Having identified a physiologically significant consequence of cell-to-cell variability in *torCAD* expression, we next wanted to determine how oxygen regulates this variability. Transcription of the *torCAD* operon is regulated by the TorT/TorS/TorR signal transduction system (Baraquet et al., 2006; Jourlin et al., 1996a, 1996b; Simon et al., 1994), which is schematized in Figure 2A. TorT and TorS function as a unit, with TorT sensing periplasmic TMAO and causing TorS to autophosphorylate. TorS-P then transfers its phosphoryl group to TorR, and TorR-P activates *torCAD* transcription. In the absence of TMAO or TorT, TorS dephosphorylates TorR-P and *torCAD* is not transcribed (Ansaldi et al., 2001; Jourlin et al., 1996b). Protein abundance measurements indicate that on average TorT and TorS are present in only a few copies per cell during aerobic growth (Li et al., 2014; Taniguchi et al., 2010), and previous work demonstrated that even modest overexpression of TorT and TorS significantly decreases variability in *torCAD* transcription (Roggiani and Goulian, 2015). Taken together, these findings suggest a model in which aerobic variability in *torCAD* expression results from the high cell-to-cell variability in the relative amounts of TorT to TorS that would be expected to occur if the molecules are on average in very low abundance (Figure 2B and S2) (see also Roggiani and Goulian, 2015). Because *torCAD* variability is greatly diminished in anaerobic conditions, we predicted higher expression of *torT* and *torS* in the absence of oxygen than in the presence of oxygen. To compare aerobic and anaerobic expression of *torT* and *torS*, we constructed fluorescent reporters as operon (transcriptional) fusions at the native *torT* and *torS* loci,

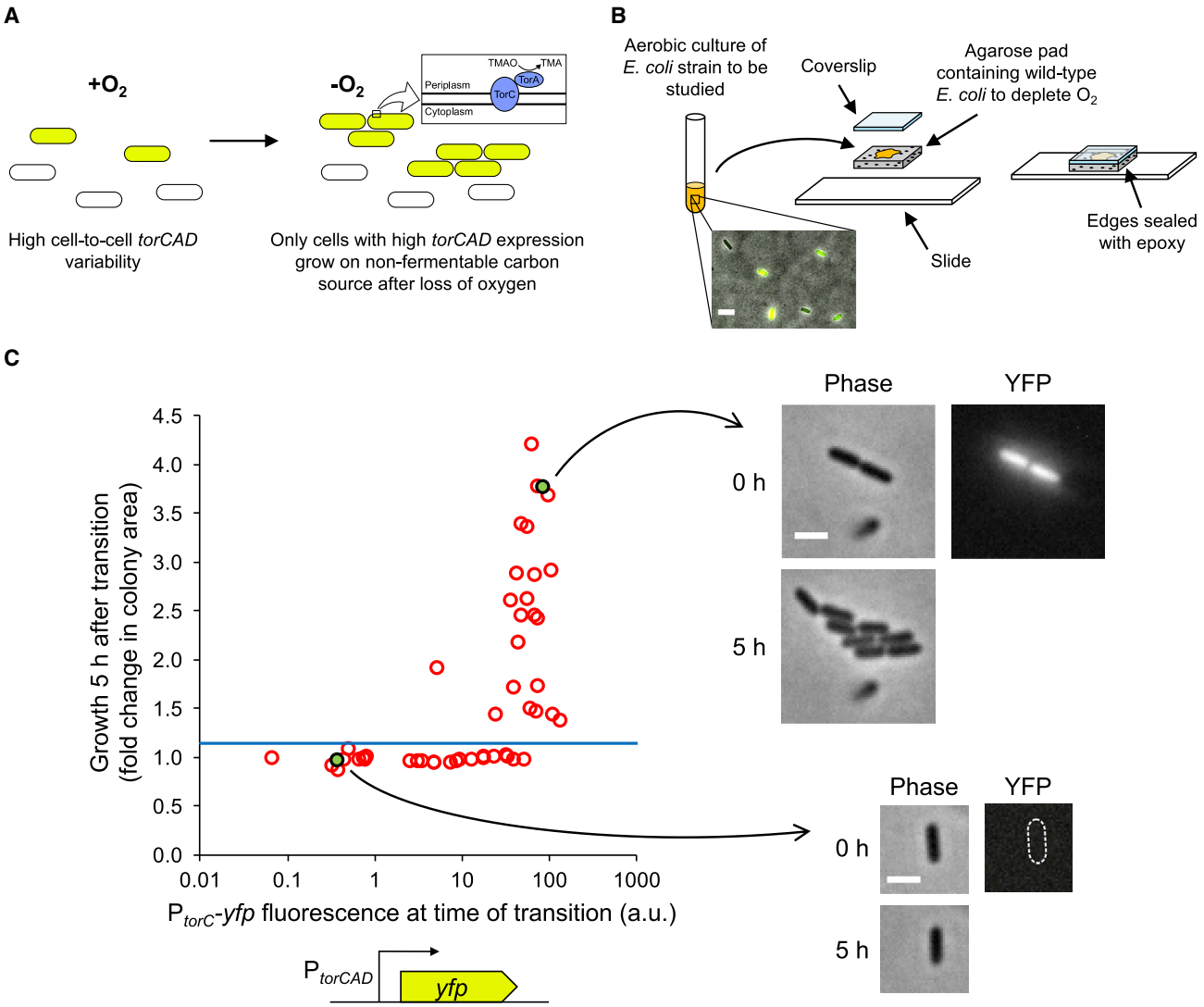

Figure 1. Cell-to-Cell Variability in *torCAD* Expression Permits a Subpopulation to Continue Growth through a Transition to Anaerobiosis

(A) For cells growing on a non-fermentable carbon source, only those cells that have recently expressed *torCAD* at a high level (green shading) are expected to grow after O_2 depletion. Inset: growth by respiration of TMAO requires the TorC and TorA proteins.

(B) Experimental setup to observe the fates of individual cells undergoing an aerobic-to-anaerobic transition. Inset: micrograph of aerobically growing *E. coli* cells harboring a P_{torCAD}-*yfp* transcriptional reporter. Scale bar, 5 μm. See Movie S1 for a time-lapse video showing P_{torCAD}-*yfp* expression in aerobically growing microcolonies.

(C) Cell growth after O_2 depletion correlates with *torCAD* expression at the time of depletion. Each circle represents a cell or microcolony of the P_{torCAD}-*yfp* P_{tetA}-*mcherry* strain MMR65. Growth is quantified as the ratio of microcolony area ~5 hr after O_2 depletion to the area of the parent cell at the time of depletion. The blue line indicates the limit of detection for cell growth. Micrographs corresponding to the green-shaded circles are indicated by arrows.

Data are shown from a single experiment, with data from a replicate experiment shown in Figure S1A. a.u., arbitrary units. Scale bars, 2 μm.

with *torT* fused to *mcherry* and *torS* fused to *yfp* (Figures 2C, S3A, and S3B). We grew the *torT-mcherry torS-yfp* reporter strain in aerobic or anaerobic conditions and used fluorescence microscopy to measure the very low cellular levels of mCherry and YFP fluorescence. Because mCherry and YFP fluorophores require oxygen for maturation (Shaner et al., 2005), early exponential phase cultures were treated with a translation inhibitor and aerated prior to fluorescence measurements. These measurements revealed that anaerobic expression of *torT* and *torS* is elevated compared to aerobic expression (Figure 2C), suggesting a higher abundance of TorT and TorS protein in anaerobically growing cells than in aerobically growing cells. We verified this result using *lacZ* reporters of *torT* and *torS* transcription, which do not require exposure to oxygen for reporter maturation (Figures S3C and S3D).

The Transcription Factor IscR Binds to *torT-torS* Intergenic Sequence

The *torT* and *torS* genes are divergently transcribed from adjacent promoters in an 82-bp intergenic region. To our knowledge,

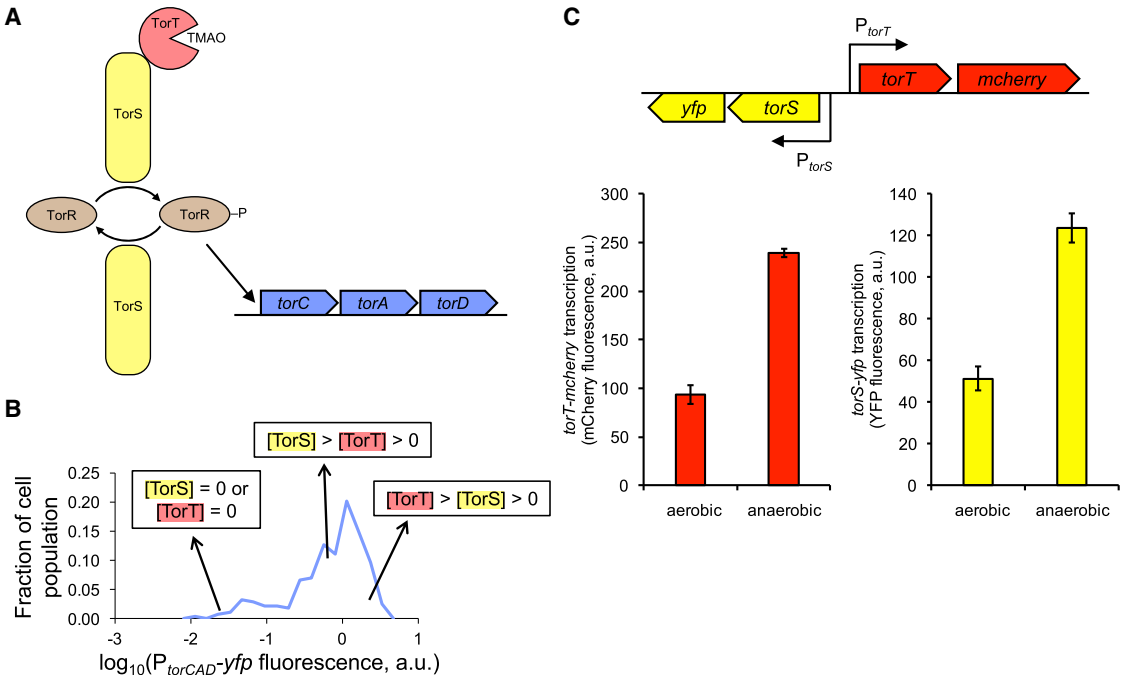

Figure 2. TorT/TorS/TorR Signaling Regulates *torCAD* Transcription, and Transcription of *torT* and *torS* is O_2-Dependent

(A) TorR is either phosphorylated or dephosphorylated by TorS depending on whether or not TorS is interacting with TorT-TMAO. TorR-P activates transcription of the *torCAD* operon.

(B) Illustration of our model as applied to the distribution of P_{torCAD}-*yfp* transcription in aerobically growing cells (data taken from Figure 5). Because aerobic TorT and TorS abundance is very low, small differences in the number of TorT and TorS molecules in an individual cell have a large effect on the concentration of TorR-P. This results in highly variable expression from the *torCAD* promoter. See Figure S2 for a simulation of the model.

(C) Operon fusions of *yfp* and *mcherry* at the *torS-torT* locus (strain JNC100) were used to measure *torS* and *torT* expression.

Bar heights represent the mean values for three independent experiments, and error bars represent SD. a.u., arbitrary units. See also Figure S3.

no regulators of *torT* or *torS* expression have been either reported or predicted, so we sought to identify transcription factors that bind in the *torT-torS* promoter region and that could account for the oxygen regulation of these two genes. Previous studies have failed to detect binding of the canonical oxygen-dependent regulators ArcA or FNR in the *torT-torS* promoter region (Myers et al., 2013; Park et al., 2013). However, chromatin immunoprecipitation sequencing (ChIP-seq) with IscR, an oxygen-sensitive transcription factor that regulates iron-sulfur (Fe-S) cluster biosynthesis (Giel et al., 2006, 2013; Schwartz et al., 2001; Vinella et al., 2013), revealed binding of IscR to the *torT-torS* promoter region that was enriched in aerobic versus anaerobic culture (Figure 3A). This observation suggested that IscR might act directly at the promoters for *torT* and/or *torS* by repressing transcription in aerobically growing cells.

Consistent with this hypothesized role for IscR, transcriptional profiling of aerobically and anaerobically growing cells with or without *iscR* revealed that *torT* and *torS* transcript abundance depended on oxygen only in the wild-type strain (Figure 3A). During aerobic growth, the wild-type strain had fewer transcripts than during anaerobic growth (in agreement with the fluorescent reporter data shown in Figure 2C). Transcript abundance in the Δ*iscR* strain was unaffected by oxygen and was the same as in the anaerobically grown wild-type strain, supporting the premise that IscR is an oxygen-sensitive repressor of *torT* and *torS* expression. A comparison of ChIP-seq data for the σ^{70} component of RNA polymerase from Myers et al. (2013) with the IscR data revealed an inverse relationship between σ^{70} binding and IscR binding (Figure 3A), further supporting the model that IscR represses transcription of *torT* and *torS* and suggests that it does so via steric inhibition of σ^{70} binding. IscR abundance is elevated during aerobic growth (Giel et al., 2013), which is consistent with the increased binding of IscR between *torT* and *torS* revealed by ChIP-seq and supports the mechanism of IscR regulation of *torT* and *torS* outlined in Figure 3B.

The IscR binding site between *torT* and *torS*, denoted b_{IscR}, was identified as a type 2 site by sequence similarity with other sites of this class. Type 2 sites can bind both holo-IscR (IscR with its Fe-S cluster) and the apo (Fe-S clusterless) form, whereas type 1 sites bind only holo-IscR (Nesbit et al., 2009). To confirm that b_{IscR} is a type 2 site and to assess the specificity and affinity of IscR binding to this sequence, we assayed IscR binding *in vitro* by fluorescence anisotropy. We performed DNA binding titration experiments using purified IscR-C92A, an IscR mutant that cannot assemble with an Fe-S cluster and is therefore only in the apo form. We characterized IscR-C92A binding to b_{IscR}, b_{IscR}^{*} (a mutant b_{IscR} sequence with a C-to-G substitution at a highly conserved cytosine in the binding site motif [Figures 3C and S4]), a known type 2 binding site sequence, and a shuffled DNA sequence (Figure 3D). As is

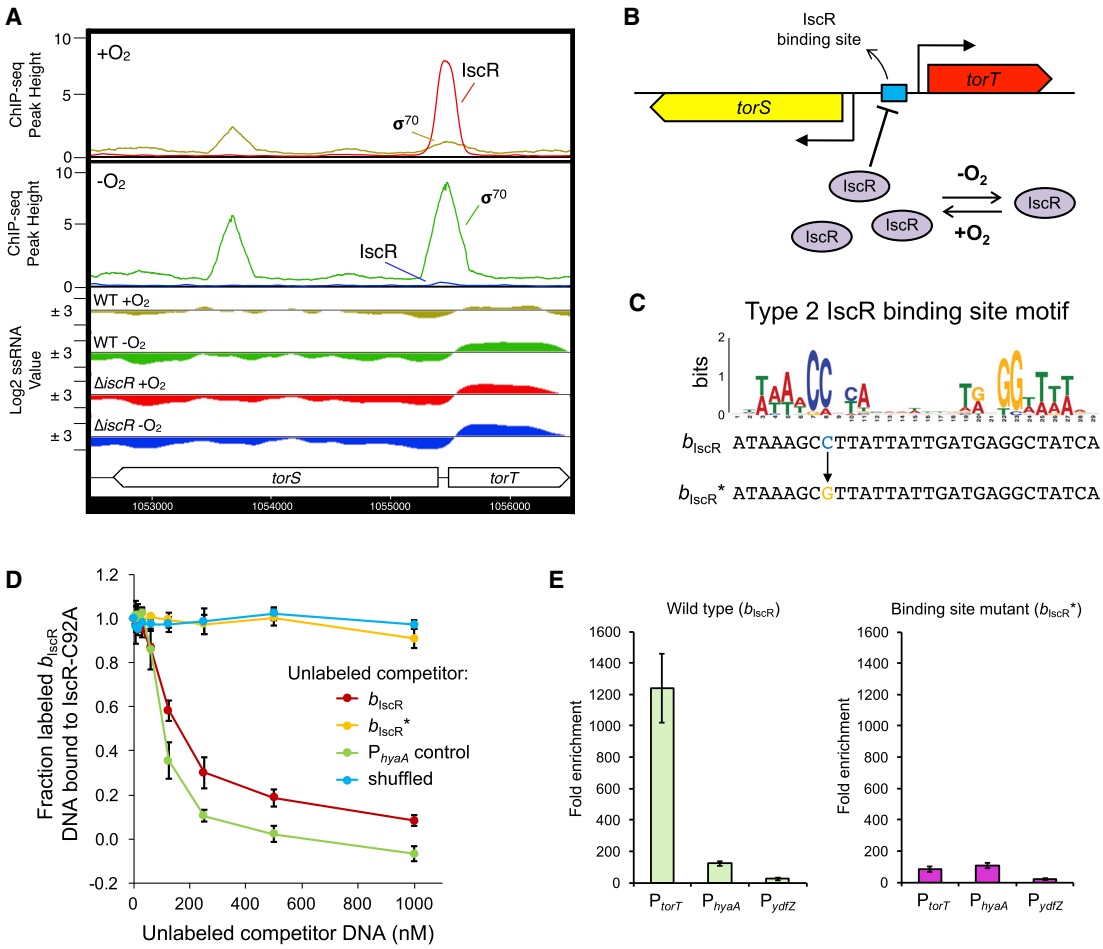

Figure 3. IscR Binds in the *torS-torT* Intergenic Region

(A) ChIP-seq for IscR in wild-type cells (MG1655) grown aerobically and anaerobically shows IscR binding between *torT* and *torS* that is elevated during aerobic growth. ChIP-seq data for σ^{70} (Myers et al., 2013) are also displayed, showing an inverse relationship between IscR and σ^{70} binding. The σ^{70} binding within the *torS* coding sequence may indicate the presence of an uncharacterized promoter. Strand-specific transcription (ssRNA) data show increased transcription of *torT* and *torS* in anaerobically growing wild-type cells (MG1655) as compared to aerobically growing cells. A strain lacking *iscR* (PK4854) shows elevated *torT* and *torS* transcription during both anaerobic and aerobic growth.

(B) Model of IscR repression of *torT* and *torS* transcription. IscR is more abundant during aerobic growth, leading to more binding between *torT* and *torS* and stronger repression than during anaerobic growth.

(C) Alignment of the sequence logo of the IscR binding site motif with the inferred IscR binding site sequence near the *torT* promoter (denoted b_{IscR}). The point mutation designated b_{IscR}* is a C-to-G mutation in the IscR binding site at position −21 relative to the start codon of *torT*. See Figure S4 for a sequence comparison among *Enterobacteriaceae*.

(D) Fluorescence anisotropy measurements show that IscR-C92A binds *in vitro* to the b_{IscR} sequence but not to the b_{IscR}* sequence. IscR-C92A was incubated with fluorescently labeled b_{IscR} DNA, and increasing amounts of unlabeled competitor DNA were added. The *hyaA* promoter is a positive control for IscR-C92A binding, and shuffled DNA is a control for nonspecific binding. Error bars represent the SDs of three experiments. The concentration of unlabeled DNA required to decrease maximum anisotropy by a factor of 0.5 (IC_{50}) is 145 ± 26 nM for the b_{IscR} sequence and 106 ± 10 nM for the *hyaA* IscR binding site sequence (mean ± SD for 3 independent experiments).

(E) ChIP-qPCR using anti-IscR antibody in a wild-type strain (MG1655, left) and a b_{IscR}*-containing strain (JNC122, right). The DNA segments targeted for quantification were the promoter regions of *torT* (containing b_{IscR} or b_{IscR}*), *hyaA* (a positive control for IscR binding), and *ydfZ* (a negative control for IscR binding). Fold enrichment indicates the ratio of ChIP-qPCR signal to no-antibody control.

Bar heights represent mean values for 3 independent experiments, and error bars represent SDs.

evident in Figure 3D, IscR-C92A binds to b_{IscR} and the known type 2 sequence but does not bind to b_{IscR}* or the shuffled sequence. We also performed ChIP-qPCR to further confirm that, *in vivo*, IscR binds the promoter region between *torS* and *torT* and that binding is greatly diminished in a strain with the b_{IscR}* mutation (Figure 3E).

IscR Regulates *torT* and *torS* Expression in an Oxygen-Dependent Manner

To test whether IscR binding in the *torT-torS* intergenic region regulates *torT* and/or *torS* expression, we first constructed an in-frame deletion of the *iscR* gene and measured *torT-mcherry* and *torS-yfp* reporter fluorescence. Expression of both genes

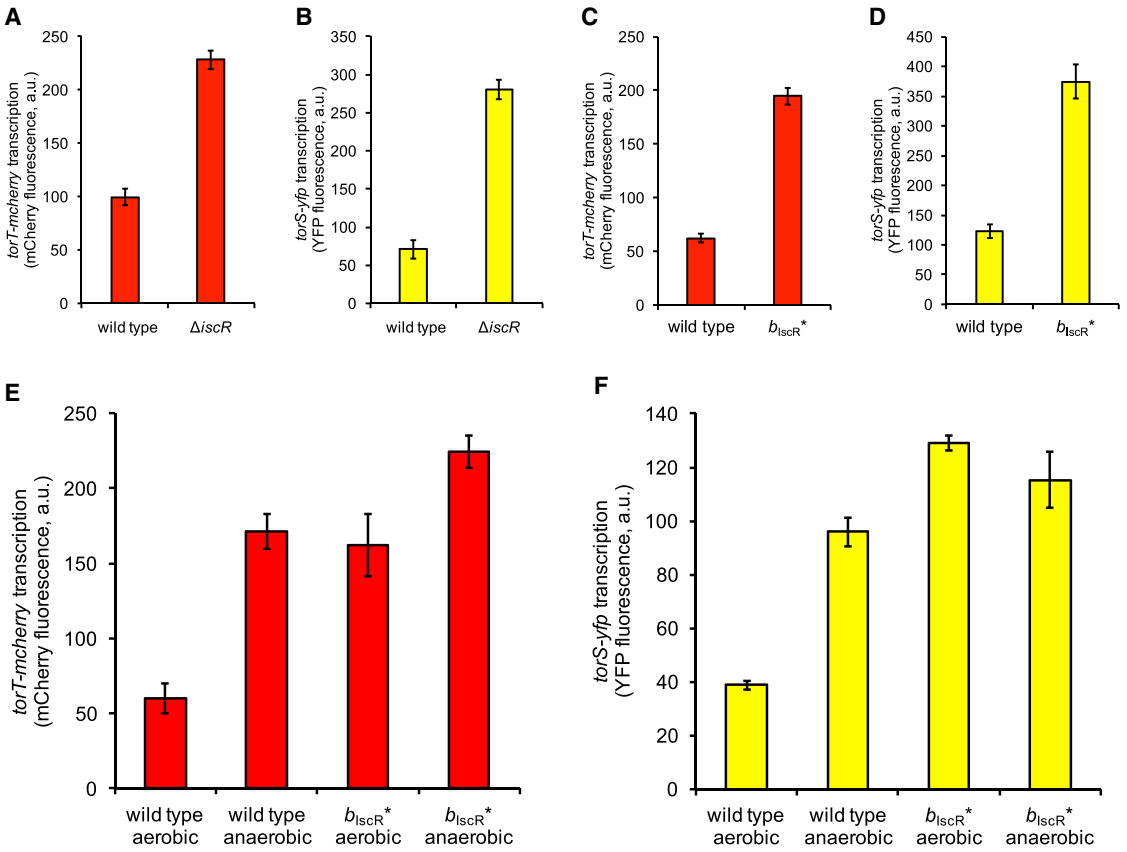

Figure 4. IscR Represses *torT* and *torS* Transcription

(A–F) Deletion of *iscR* increases aerobic transcription of (A) *torT* and (B) *torS*. Transcription of (C) *torT* and (D) *torS* is increased in strains harboring the b_{IscR}* IscR binding site mutation. Oxygen regulation of (E) *torT* and (F) *torS* expression is disrupted in b_{IscR}*-containing strains.

Bar heights represent the mean values for three independent experiments, and error bars represent SDs. a.u., arbitrary units. Reporter strains were JNC100, JNC104 (A and B) and JNC92, JNC115, JNC73, and JNC112 (C–F). See also Figure S5.

was elevated in the Δ*iscR* strain relative to the wild-type strain (Figures 4A and 4B), which is consistent with the transcriptional profiling results (Figure 3A) and indicates that IscR represses transcription of both *torT* and *torS*.

Because IscR is a global regulator and its deletion might have an indirect effect on numerous cellular functions, we also tested the effect of the IscR binding site mutation b_{IscR}*. By measuring aerobic *torT* and *torS* transcription via the *torT-mcherry* and *torS-yfp* constructs, we found that strains containing b_{IscR}* have elevated *torT* and *torS* expression relative to strains with wild-type b_{IscR} (Figures 4C and 4D), and the fold increase of *torT* and *torS* expression is nearly the same in b_{IscR}* and Δ*iscR* strains. Furthermore, the deletion of *iscR* in b_{IscR}* strains has little additional effect on *torT* and *torS* expression (Figure S5). Taken together, these results support the proposed role of IscR as a repressor of *torT* and *torS* expression. We also note that the results in Figure S5 indicate that the b_{IscR}* mutation has little effect on the basal transcription from the *torT* and *torS* promoters.

To test whether IscR's regulation of *torT* and *torS* expression is oxygen-dependent, we compared aerobic and anaerobic expression of *torT* and *torS* in wild-type and b_{IscR}* strains (Figures 4E and 4F). While transcription of *torT* and *torS* in wild-type strains is increased in anaerobic compared to aerobic conditions (see also Figure 2C), transcription of *torT* and *torS* in the b_{IscR}* strains is similar in both conditions. There may be some degree of IscR-independent, oxygen-dependent regulation of *torT* transcription (Figure 4E), but most of the oxygen-dependent regulation appears to occur through the action of IscR.

IscR Regulates Variability in *torCAD* Expression through Oxygen-Dependent Repression of *torS* and *torT* Transcription

We next examined whether eliminating the repression of *torT* and *torS* transcription by IscR could suppress cell-to-cell variability in *torCAD* expression. Using a P_{torCAD}-*yfp* reporter strain, we found that variability in *torCAD* transcription is greatly diminished in a Δ*iscR* background (Figure 5). Unexpectedly, we found that deleting *iscR* also decreases mean *torCAD* expression (Figure 5, inset). We do not know the explanation for this effect on the mean, but we suspect that it may be due to inefficient maturation of the TorC cytochrome *c* caused by deletion of *iscR*, as apo-TorC lowers *torCAD* expression by inhibiting TorS kinase activity (Ansaldi et al., 1999; Gon et al., 2001). Consistent with this explanation, we found that deleting *torC* increases transcription

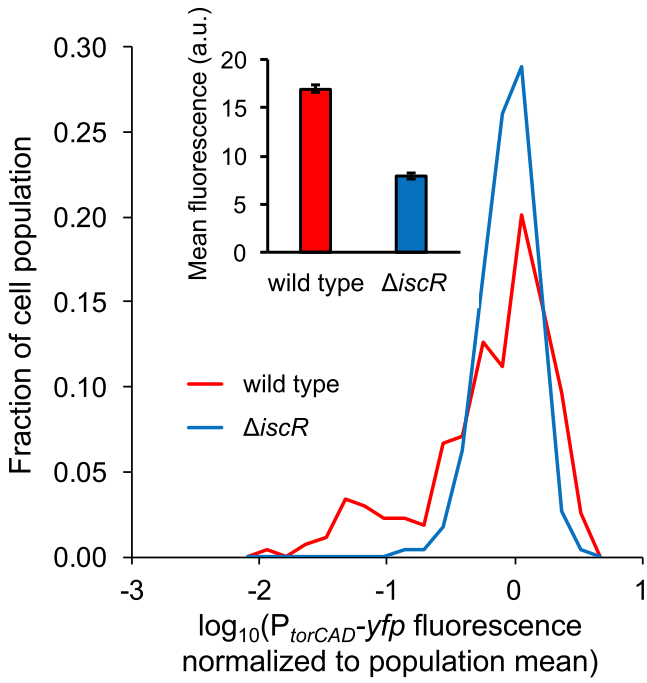

Figure 5. Deletion of *iscR* Suppresses Variability in Aerobic *torCAD* Transcription

The plot shows the distributions of single-cell fluorescence for wild-type and Δ*iscR* strains (MMR8 and MMR210). Single-cell fluorescence was quantified as YFP fluorescence normalized by a CFP internal standard (Roggiani and Goulian, 2015). Values on the x axis are expressed as fluorescence normalized by the mean value from the corresponding dataset. Each dataset consists of combined measurements from two independent experiments. Inset: mean fluorescence for the datasets shown in the main plot. Bar heights represent the mean values for two independent experiments, and error bars represent the ranges. a.u., arbitrary units.

See also Figure S6.

from the *torCAD* promoter (Figure S6). However, we note that apo-TorC does not appear to play a role in regulating variable expression from the *torCAD* promoter, as deletion of *torC* has no effect on variability in either aerobic or anaerobic conditions (Figure S6).

We also found that introducing the IscR binding site mutation b_{IscR}* decreases cell-to-cell variability in *torCAD* transcription, conferring the same low variability phenotype found in wild-type cells under anaerobic conditions (Figure 6A). Thus, cells with the b_{IscR}* mutation are effectively blind to oxygen with respect to *torCAD* transcription. Furthermore, the mean *torCAD* expression level is relatively uniform between wild-type and b_{IscR}* strains (Figure 6B), which differs from the decreased *torCAD* expression seen in the Δ*iscR* strains (Figure 5). We attribute this to the fact that IscR protein is still present in the b_{IscR}* mutant strain and can fulfill its other regulatory roles.

To investigate the physiological impact of low variability of *torCAD* transcription under aerobic conditions, we repeated the aerobic-to-anaerobic transition experiment shown in Figure 1C but this time using a P_{torCAD}-*yfp* reporter strain that has the b_{IscR}* mutation. A plot of cell growth against YFP fluorescence at the time of oxygen depletion shows that nearly every cell continues to grow after oxygen depletion (Figure 7 and S7). These results suggest that in the absence of IscR repression of *torS* and *torT*, most of the cells in the population have sufficient TorC and TorA to effectively transition to anaerobic TMAO respiration.

DISCUSSION

TMAO can be found in a number of natural environments (Barrett and Kwan, 1985; Stella et al., 2006; Wang et al., 2014). In the context of animal hosts, which are generally considered to be the primary habitat for *E. coli* (Tenaillon et al., 2010), TMAO may be directly ingested from the diet, particularly from seafood (Mitchell et al., 2002; Zhang et al., 1999), and may also be produced endogenously in the gut through host processes (Rivera-Chávez and Bäumler, 2015; Winter et al., 2013a, 2013b). Data on the concentration of TMAO in the intestine are generally lacking, but some human metabolomic studies have reported fecal TMAO concentrations well within the range that induces TMAO reductase expression in *E. coli* (Di Cagno et al., 2011; Francavilla et al., 2012; Roggiani and Goulian, 2015).

We hypothesize that the cell-to-cell variability in aerobic *torCAD* expression has evolved to allow *E. coli* to thrive even if subjected to a sudden decrease in oxygen availability. Such rapid depletion of oxygen might occur through physical translocation of bacteria from an oxygenated to an anoxic environment (e.g., when moving from a free-living state to the mammalian gut) or through depletion of oxygen in a single environment (e.g., by consumption of oxygen by bacterial populations at high cell density). In the context of the gut environment, oxygen concentrations are extremely low in the bulk of the intestinal volume. However, spatially refined measurements have revealed the existence of a radial oxygen gradient in the intestine, with relatively high dissolved oxygen at the intestinal epithelium, an aerotolerant microbiota in the epithelium-adjacent mucosa, and a steep gradient to anaerobiosis in the lumen (Albenberg et al., 2014). Because bacterial oxygen consumption is the likely cause of this gradient, at least some intestinal bacteria are exposed to oxygen and its effects. Variability in local dissolved oxygen concentrations may also occur as a direct or indirect result of variations in the longitudinal flux and composition of luminal contents in the intestine. Additionally, opportunities exist for *E. coli* to encounter TMAO and oxygen outside of a host. For example, urine often contains a significant amount of TMAO (Miller et al., 2014; Stubbs et al., 2016; Zhang et al., 1999), and growth to high cell densities in environments contaminated with urine would likely have a significant impact on the duration and magnitude of oxygen exposure.

An outstanding question regarding the regulatory mechanism described here concerns the cost of aerobic *torCAD* expression. Presumably, there is a metabolic cost associated with synthesizing and assembling the TMAO reductase complex, particularly considering its requirement for heme and molybdenum cofactors. Indeed, it is hard to imagine why *torCAD* expression would be regulated by TMAO if the cost were negligible. It is also possible that under some conditions there is a metabolic burden from shunting electrons to reduce TMAO instead of oxygen. We have been unable to demonstrate a

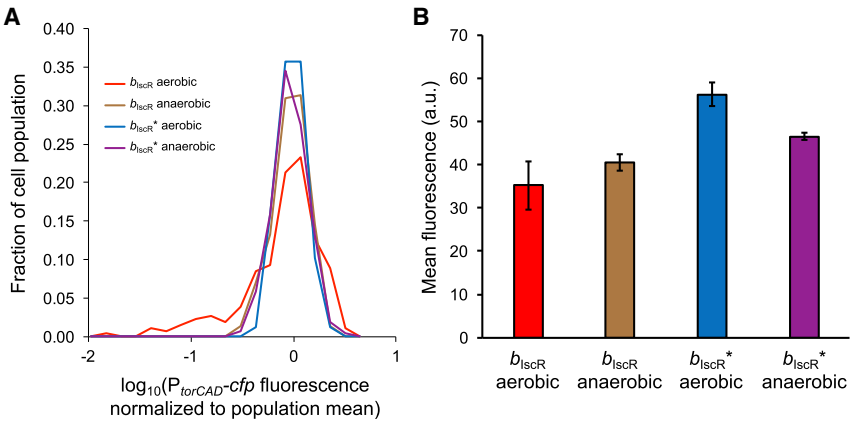

Figure 6. Variability in Aerobic *torCAD* Transcription Requires IscR Binding between *torT* and *torS* in Aerobic Conditions

(A) Distributions of aerobic and anaerobic single-cell fluorescence for wild-type and b_{IscR}* strains (JNC117 and JNC116). Single-cell fluorescence was quantified as CFP fluorescence normalized by cell area. Values on the x axis are expressed as fluorescence normalized by the mean value from the corresponding dataset. Each dataset consists of combined measurements from two independent experiments.

(B) Mean fluorescence for the data shown in (A). Bar heights represent the mean values for two independent experiments, and error bars represent the ranges. a.u., arbitrary units.

fitness cost in competition experiments between strains that uniformly express *torCAD* aerobically (via the b_{IscR}* mutation) and wild-type strains (data not shown). However, laboratory growth conditions do not necessarily reflect the evolutionary pressures that shaped the architecture and behavior of this genetic circuit, and the disadvantage of uniform expression of *torCAD* could be unmasked in conditions we have not yet explored. Additionally, the sequence-level conservation of the *torT-torS* intergenic region, and of the IscR binding site sequence in particular, is high among many members of the *Enterobacteriaceae* (Figure S4). This strongly suggests that evolutionary pressures have favored retention of the particular regulatory mechanism described in this paper along with the regulation of TorCAD synthesis in general, and that in environments where *E. coli* encounters oxygen and TMAO there is a fitness cost associated with uniform production of TorCAD that we have not yet been able to detect.

The regulation of *torCAD* variability in response to oxygen also invites consideration of several features of the TorT/TorS/TorR signaling system. First, the sensory and kinase/phosphotransfer roles belong to two separate proteins (TorT and TorS, respectively) (Baraquet et al., 2006), a feature that is also found in quorum sensing (Waters and Bassler, 2005), chemotaxis (Wadhams and Armitage, 2004), and various transport-associated signaling systems (Piepenbreier et al., 2017), among others. Second, TorT interaction with TorS determines whether TorS predominantly acts to phosphorylate or dephosphorylate TorR when TMAO is present. Third, the *torT* and *torS* genes are each expressed from their own promoter, suggesting their transcription is not tightly coupled. Finally, TorT and TorS are maintained at exceptionally low abundance in the presence of oxygen (Li et al., 2014; Taniguchi et al., 2010). Together, these features of the Tor system suggest that small differences in the number of TorT and TorS molecules between cells could result in large differences in intracellular TorR-P levels. Furthermore, at low numbers of TorT and TorS the variance in the output would be sensitive to relatively small changes in *torT* and *torS* transcription, as we have observed for aerobic versus anaerobic growth (Figure 6A). As a proof of principle, we have further demonstrated in a simple computational model that a small change in expression of these two signaling proteins can have a large effect on the output (Figure S2).

We have shown that the regulation of cell-to-cell variability by oxygen is mediated by the transcription factor IscR, which binds between *torT* and *torS* and represses transcription of both genes. IscR is more abundant during aerobic growth than during anaerobic growth (Giel et al., 2006, 2013; Mettert and Kiley, 2014), which suggests that the increased expression of *torT* and *torS* under anaerobic conditions results from decreased IscR concentration and lowers the cell-to-cell variability in *torCAD* transcription, consistent with our model and previous observations on the effects of plasmid-based expression of *torT* and *torS* (Roggiani and Goulian, 2015).

In our model of regulated cell-to-cell variability of *torCAD* expression, the amount of TorT and TorS protein produced under IscR-repressed (aerobic) conditions is low enough that stochastic effects in protein production and partitioning at cell division are important. The inverse relationship between mean protein copy number and the significance of noise has long been recognized (Bar-Even et al., 2006; Elowitz et al., 2002; Ozbudak et al., 2002; Paulsson, 2004). Low abundance of TorT and TorS creates cell-to-cell variability in the TorT/TorS ratio, and because of the division of labor between TorT (sensing TMAO) and TorS (phosphorylating and dephosphorylating TorR), the cell's TorT/TorS ratio determines the concentration of phosphorylated TorR and the magnitude of the transcriptional response to the presence of TMAO (Figure 2B). In aerobic conditions, when *torT* and *torS* are repressed, the TorT/TorS ratio can differ markedly between cells in a population exposed to the same concentration of TMAO, which leads to high cell-to-cell variability in *torCAD* expression. Anaerobically, *torT* and *torS* are derepressed, and at these higher TorT and TorS levels the TorT/TorS ratio becomes insensitive to stochasticity in gene expression and protein partitioning. Expression of *torCAD* is therefore much more uniform across the population in anaerobic conditions. One particularly interesting consequence of this mechanism for generating heterogeneity in gene expression is that individual cell lineages frequently traverse the range of *torCAD* induction: each TorT or TorS production burst and each cell division partitioning event significantly alters the concentration of TorR-P in the cell. A consequence of this behavior is that the

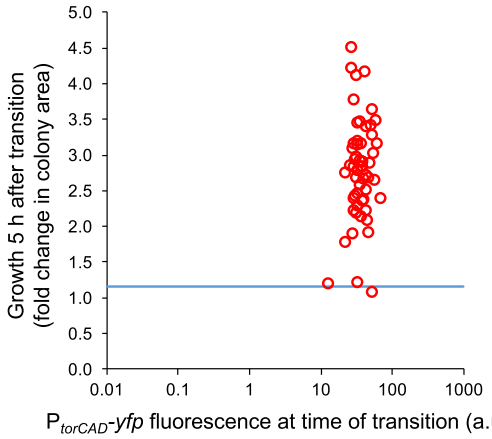

Figure 7. Uniform Expression of *torCAD* Permits Growth of Nearly the Entire Population after O_2 Depletion

Each circle represents a cell or microcolony of the P_{torCAD}-*yfp* b_{IscR}* strain JNC123. Growth is quantified as in Figure 1C. The blue line indicates the limit of detection for cell growth. Data are shown from a single experiment, with data from a replicate experiment shown in Figure S7. a.u., arbitrary units.

cost associated with low fitness states is shared by all cell lineages in the population. This property contrasts with phenotypic variability based on bistability in which "on" and "off" states are inherited over multiple generations (for reviews covering the subject, see Dubnau and Losick, 2006; Eldar and Elowitz, 2010; Losick and Desplan, 2008; Smits et al., 2006), causing specific lineages to bear most of the fitness burden. To our knowledge, the Tor system is the first reported example of cells harnessing stochasticity in cellular protein levels to regulate the variability in the output of a signaling system without changing the mean. As evolution tends to reuse effective strategies, it is likely that other biological signaling systems have evolved to regulate variability through similar mechanisms.

STAR★METHODS

Detailed methods are provided in the online version of this paper and include the following:

- KEY RESOURCES TABLE
- CONTACT FOR REAGENT AND RESOURCE SHARING
- EXPERIMENTAL MODEL AND SUBJECT DETAILS
  - Bacterial growth media and conditions
- METHOD DETAILS
  - Strain construction
  - Phase contrast and fluorescence microscopy
  - Aerobic-to-anaerobic transition microscopy
  - Time-lapse microscopy
  - β-Galactosidase assays
  - Sequence alignment
  - ChIP-seq and transcriptomics
  - DNA-binding fluorescence polarization assays
  - ChIP-qPCR analysis
  - Computer simulations
- QUANTIFICATION AND STATISTICAL ANALYSIS
- DATA AND SOFTWARE AVAILABILITY

SUPPLEMENTAL INFORMATION

Supplemental Information includes seven figures, three tables, and one movie and can be found with this article online at https://doi.org/10.1016/j.cell.2018.02.005.

ACKNOWLEDGMENTS

We are grateful to Sergei Vinogradov for reagents, equipment, and expertise in measuring oxygen concentrations and to Andrew Binns, Fevzi Daldal, Arjun Raj, Jun Zhu, E. Josie Clowney, and members of the Goulian, Binns, and Zhu labs for valuable insights and discussion. This work was funded by grants from the National Institute of General Medical Sciences of the NIH (R01-GM080279 to M.G. and R01-GM115894 to P.J.K.) and by NIH training grants (T32-AI060516 and T32-GM007170 to J.N.C.). This work was supported in part by the Penn Genome Frontiers Institute and funding from the Pennsylvania Department of Health. The Department of Health specifically disclaims responsibility for any analysis, interpretations, or conclusions. Additional funding was provided by the Armour-Lewis Foundation and the Dean's Office of the University of Pennsylvania School of Veterinary Medicine.

AUTHOR CONTRIBUTIONS

All authors conceived experiments, designed methodology. conducted experiments, and performed data analysis. J.N.C. developed the computer simulation. J.N.C. and M.G. wrote the manuscript. All authors contributed to manuscript revisions and editing.

DECLARATION OF INTERESTS

The authors declare no competing interests.

Received: July 6, 2017
Revised: December 1, 2017
Accepted: February 1, 2018
Published: March 1, 2018

SUPPORTING CITATIONS

The following references appear in the Supplemental Information: Batchelor and Goulian (2006); Libby et al. (2010).

REFERENCES

Ackermann, M., Stecher, B., Freed, N.E., Songhet, P., Hardt, W.D., and Doebeli, M. (2008). Self-destructive cooperation mediated by phenotypic noise. Nature *454*, 987–990.

Albenberg, L., Esipova, T.V., Judge, C.P., Bittinger, K., Chen, J., Laughlin, A., Grunberg, S., Baldassano, R.N., Lewis, J.D., Li, H., et al. (2014). Correlation between intraluminal oxygen gradient and radial partitioning of intestinal microbiota. Gastroenterology *147*, 1055–1063.

Ansaldi, M., Bordi, C., Lepelletier, M., and Méjean, V. (1999). TorC apocytochrome negatively autoregulates the trimethylamine N-oxide (TMAO) reductase operon in Escherichia coli. Mol. Microbiol. *33*, 284–295.

Ansaldi, M., Jourlin-Castelli, C., Lepelletier, M., Théraulaz, L., and Méjean, V. (2001). Rapid dephosphorylation of the TorR response regulator by the TorS unorthodox sensor in Escherichia coli. J. Bacteriol. *183*, 2691–2695.

Ansaldi, M., Théraulaz, L., Baraquet, C., Panis, G., and Méjean, V. (2007). Aerobic TMAO respiration in Escherichia coli. Mol. Microbiol. *66*, 484–494.

Baba, T., Ara, T., Hasegawa, M., Takai, Y., Okumura, Y., Baba, M., Datsenko, K.A., Tomita, M., Wanner, B.L., and Mori, H. (2006). Construction of Escherichia coli K-12 in-frame, single-gene knockout mutants: the Keio collection. Mol. Syst. Biol. *2*, 2006.0008.

Balaban, N.Q., Merrin, J., Chait, R., Kowalik, L., and Leibler, S. (2004). Bacterial persistence as a phenotypic switch. Science *305*, 1622–1625.

Bar-Even, A., Paulsson, J., Maheshri, N., Carmi, M., O'Shea, E., Pilpel, Y., and Barkai, N. (2006). Noise in protein expression scales with natural protein abundance. Nat. Genet. *38*, 636–643.

Baraquet, C., Théraulaz, L., Guiral, M., Lafitte, D., Méjean, V., and Jourlin-Castelli, C. (2006). TorT, a member of a new periplasmic binding protein family, triggers induction of the Tor respiratory system upon trimethylamine N-oxide electron-acceptor binding in Escherichia coli. J. Biol. Chem. *281*, 38189–38199.

Barrett, E.L., and Kwan, H.S. (1985). Bacterial reduction of trimethylamine oxide. Annu. Rev. Microbiol. *39*, 131–149.

Batchelor, E., and Goulian, M. (2006). Imaging OmpR localization in Escherichia coli. Mol. Microbiol. *59*, 1767–1778.

Blank, K., Hensel, M., and Gerlach, R.G. (2011). Rapid and highly efficient method for scarless mutagenesis within the Salmonella enterica chromosome. PLoS ONE *6*, e15763.

Boratyn, G.M., Camacho, C., Cooper, P.S., Coulouris, G., Fong, A., Ma, N., Madden, T.L., Matten, W.T., McGinnis, S.D., Merezhuk, Y., et al. (2013). BLAST: a more efficient report with usability improvements. Nucleic Acids Res. *41*, W29–33.

Cherepanov, P.P., and Wackernagel, W. (1995). Gene disruption in Escherichia coli: TcR and KmR cassettes with the option of Flp-catalyzed excision of the antibiotic-resistance determinant. Gene *158*, 9–14.

Cho, B.K., Zengler, K., Qiu, Y., Park, Y.S., Knight, E.M., Barrett, C.L., Gao, Y., and Palsson, B.Ø. (2009). The transcription unit architecture of the Escherichia coli genome. Nat. Biotechnol. *27*, 1043–1049.

Datsenko, K.A., and Wanner, B.L. (2000). One-step inactivation of chromosomal genes in Escherichia coli K-12 using PCR products. Proc. Natl. Acad. Sci. USA *97*, 6640–6645.

Davis, S.E., Mooney, R.A., Kanin, E.I., Grass, J., Landick, R., and Ansari, A.Z. (2011). Mapping E. coli RNA polymerase and associated transcription factors and identifying promoters genome-wide. Methods Enzymol. *498*, 449–471.

Di Cagno, R., De Angelis, M., De Pasquale, I., Ndagijimana, M., Vernocchi, P., Ricciuti, P., Gagliardi, F., Laghi, L., Crecchio, C., Guerzoni, M.E., et al. (2011). Duodenal and faecal microbiota of celiac children: molecular, phenotype and metabolome characterization. BMC Microbiol. *11*, 219.

Dubnau, D., and Losick, R. (2006). Bistability in bacteria. Mol. Microbiol. *61*, 564–572.

Ducret, A., Quardokus, E.M., and Brun, Y.V. (2016). MicrobeJ, a tool for high throughput bacterial cell detection and quantitative analysis. Nat. Microbiol. *1*, 16077.

El Meouche, I., Siu, Y., and Dunlop, M.J. (2016). Stochastic expression of a multiple antibiotic resistance activator confers transient resistance in single cells. Sci. Rep. *6*, 19538.

Eldar, A., and Elowitz, M.B. (2010). Functional roles for noise in genetic circuits. Nature *467*, 167–173.

Elowitz, M.B., Levine, A.J., Siggia, E.D., and Swain, P.S. (2002). Stochastic gene expression in a single cell. Science *297*, 1183–1186.

Francavilla, R., Calasso, M., Calace, L., Siragusa, S., Ndagijimana, M., Vernocchi, P., Brunetti, L., Mancino, G., Tedeschi, G., Guerzoni, E., et al. (2012). Effect of lactose on gut microbiota and metabolome of infants with cow's milk allergy. Pediatr. Allergy Immunol. *23*, 420–427.

Friedman, N., Cai, L., and Xie, X.S. (2006). Linking stochastic dynamics to population distribution: an analytical framework of gene expression. Phys. Rev. Lett. *97*, 168302.

Giel, J.L., Rodionov, D., Liu, M., Blattner, F.R., and Kiley, P.J. (2006). IscR-dependent gene expression links iron-sulphur cluster assembly to the control of O2-regulated genes in Escherichia coli. Mol. Microbiol. *60*, 1058–1075.

Giel, J.L., Nesbit, A.D., Mettert, E.L., Fleischhacker, A.S., Wanta, B.T., and Kiley, P.J. (2013). Regulation of iron-sulphur cluster homeostasis through transcriptional control of the Isc pathway by [2Fe-2S]-IscR in Escherichia coli. Mol. Microbiol. *87*, 478–492.

Gon, S., Jourlin-Castelli, C., Théraulaz, L., and Méjean, V. (2001). An unsuspected autoregulatory pathway involving apocytochrome TorC and sensor TorS in Escherichia coli. Proc. Natl. Acad. Sci. USA *98*, 11615–11620.

Hassan, J., Bergaust, L.L., Wheat, I.D., and Bakken, L.R. (2014). Low probability of initiating nirS transcription explains observed gas kinetics and growth of bacteria switching from aerobic respiration to denitrification. PLoS Comput. Biol. *10*, e1003933.

Irizarry, R.A., Bolstad, B.M., Collin, F., Cope, L.M., Hobbs, B., and Speed, T.P. (2003). Summaries of Affymetrix GeneChip probe level data. Nucleic Acids Res. *31*, e15.

Jourlin, C., Bengrine, A., Chippaux, M., and Méjean, V. (1996a). An unorthodox sensor protein (TorS) mediates the induction of the tor structural genes in response to trimethylamine N-oxide in Escherichia coli. Mol. Microbiol. *20*, 1297–1306.

Jourlin, C., Simon, G., Pommier, J., Chippaux, M., and Méjean, V. (1996b). The periplasmic TorT protein is required for trimethylamine N-oxide reductase gene induction in Escherichia coli. J. Bacteriol. *178*, 1219–1223.

Khodursky, A.B., Bernstein, J.A., Peter, B.J., Rhodius, V., Wendisch, V.F., and Zimmer, D.P. (2003). Escherichia coli spotted double-strand DNA microarrays: RNA extraction, labeling, hybridization, quality control, and data management. Methods Mol. Biol. *224*, 61–78.

Kotte, O., Volkmer, B., Radzikowski, J.L., and Heinemann, M. (2014). Phenotypic bistability in Escherichia coli's central carbon metabolism. Mol. Syst. Biol. *10*, 736.

Kussell, E., and Leibler, S. (2005). Phenotypic diversity, population growth, and information in fluctuating environments. Science *309*, 2075–2078.

Lebedev, A.Y., Cheprakov, A.V., Sakadzić, S., Boas, D.A., Wilson, D.F., and Vinogradov, S.A. (2009). Dendritic phosphorescent probes for oxygen imaging in biological systems. ACS Appl. Mater. Interfaces *1*, 1292–1304.

Levy, S.F., Ziv, N., and Siegal, M.L. (2012). Bet hedging in yeast by heterogeneous, age-correlated expression of a stress protectant. PLoS Biol. *10*, e1001325.

Li, G.W., Burkhardt, D., Gross, C., and Weissman, J.S. (2014). Quantifying absolute protein synthesis rates reveals principles underlying allocation of cellular resources. Cell *157*, 624–635.

Libby, E.A., Ekici, S., and Goulian, M. (2010). Imaging OmpR binding to native chromosomal loci in Escherichia coli. J. Bacteriol. *192*, 4045–4053.

Losick, R., and Desplan, C. (2008). Stochasticity and cell fate. Science *320*, 65–68.

Maisonneuve, E., and Gerdes, K. (2014). Molecular mechanisms underlying bacterial persisters. Cell *157*, 539–548.

Maslov, S., and Sneppen, K. (2015). Well-temperate phage: optimal bet-hedging against local environmental collapses. Sci. Rep. *5*, 10523.

McCrindle, S.L., Kappler, U., and McEwan, A.G. (2005). Microbial dimethylsulfoxide and trimethylamine-N-oxide respiration. Adv. Microb. Physiol. *50*, 147–198.

Méjean, V., Iobbi-Nivol, C., Lepelletier, M., Giordano, G., Chippaux, M., and Pascal, M.C. (1994). TMAO anaerobic respiration in Escherichia coli: involvement of the tor operon. Mol. Microbiol. *11*, 1169–1179.

Mettert, E.L., and Kiley, P.J. (2014). Coordinate regulation of the Suf and Isc Fe-S cluster biogenesis pathways by IscR is essential for viability of Escherichia coli. J. Bacteriol. *196*, 4315–4323.

Miller, J.H. (1992). A Short Course in Bacterial Genetics: A Laboratory Manual and Handbook for Escherichia coli and Related Bacteria (Cold Spring Harbor Laboratory Press).

Miller, C.A., Corbin, K.D., da Costa, K.A., Zhang, S., Zhao, X., Galanko, J.A., Blevins, T., Bennett, B.J., O'Connor, A., and Zeisel, S.H. (2014). Effect of egg ingestion on trimethylamine-N-oxide production in humans: a randomized, controlled, dose-response study. Am. J. Clin. Nutr. *100*, 778–786.

Mitchell, S.C., Zhang, A.Q., and Smith, R.L. (2002). Chemical and biological liberation of trimethylamine from foods. J. Food Compos. Anal. *15*, 277–282.

Miyashiro, T., and Goulian, M. (2007). Single-cell analysis of gene expression by fluorescence microscopy. Methods Enzymol. *423*, 458–475.

Myers, K.S., Yan, H., Ong, I.M., Chung, D., Liang, K., Tran, F., Keleş, S., Landick, R., and Kiley, P.J. (2013). Genome-scale analysis of escherichia coli FNR reveals complex features of transcription factor binding. PLoS Genet. *9*, e1003565.

Neidhardt, F.C., Bloch, P.L., and Smith, D.F. (1974). Culture medium for enterobacteria. J. Bacteriol. *119*, 736–747.

Nesbit, A.D., Giel, J.L., Rose, J.C., and Kiley, P.J. (2009). Sequence-specific binding to a subset of IscR-regulated promoters does not require IscR Fe-S cluster ligation. J. Mol. Biol. *387*, 28–41.

Nesbit, A.D., Fleischhacker, A.S., Teter, S.J., and Kiley, P.J. (2012). ArcA and AppY antagonize IscR repression of hydrogenase-1 expression under anaerobic conditions, revealing a novel mode of O2 regulation of gene expression in Escherichia coli. J. Bacteriol. *194*, 6892–6899.

Nielsen, A.T., Dolganov, N.A., Rasmussen, T., Otto, G., Miller, M.C., Felt, S.A., Torreilles, S., and Schoolnik, G.K. (2010). A bistable switch and anatomical site control Vibrio cholerae virulence gene expression in the intestine. PLoS Pathog. *6*, e1001102.

Notredame, C., Higgins, D.G., and Heringa, J. (2000). T-Coffee: A novel method for fast and accurate multiple sequence alignment. J. Mol. Biol. *302*, 205–217.

Ozbudak, E.M., Thattai, M., Kurtser, I., Grossman, A.D., and van Oudenaarden, A. (2002). Regulation of noise in the expression of a single gene. Nat. Genet. *31*, 69–73.

Ozbudak, E.M., Thattai, M., Lim, H.N., Shraiman, B.I., and Van Oudenaarden, A. (2004). Multistability in the lactose utilization network of Escherichia coli. Nature *427*, 737–740.

Park, D.M., Akhtar, M.S., Ansari, A.Z., Landick, R., and Kiley, P.J. (2013). The bacterial response regulator ArcA uses a diverse binding site architecture to regulate carbon oxidation globally. PLoS Genet. *9*, e1003839.

Paulsson, J. (2004). Summing up the noise in gene networks. Nature *427*, 415–418.

Piepenbreier, H., Fritz, G., and Gebhard, S. (2017). Transporters as information processors in bacterial signalling pathways. Mol. Microbiol. *104*, 1–15.

Pommier, J., Méjean, V., Giordano, G., and Iobbi-Nivol, C. (1998). TorD, a cytoplasmic chaperone that interacts with the unfolded trimethylamine N-oxide reductase enzyme (TorA) in Escherichia coli. J. Biol. Chem. *273*, 16615–16620.

Rajagopalan, S., Teter, S.J., Zwart, P.H., Brennan, R.G., Phillips, K.J., and Kiley, P.J. (2013). Studies of IscR reveal a unique mechanism for metal-dependent regulation of DNA binding specificity. Nat. Struct. Mol. Biol. *20*, 740–747.

Ratcliff, W.C., and Denison, R.F. (2010). Individual-level bet hedging in the bacterium Sinorhizobium meliloti. Curr. Biol. *20*, 1740–1744.

Rivera-Chávez, F., and Bäumler, A.J. (2015). The pyromaniac inside you: Salmonella metabolism in the host gut. Annu. Rev. Microbiol. *69*, 31–48.

Roggiani, M., and Goulian, M. (2015). Oxygen-dependent cell-to-cell variability in the output of the Escherichia coli Tor phosphorelay. J. Bacteriol. *197*, 1976–1987.

Rouzine, I.M., Weinberger, A.D., and Weinberger, L.S. (2015). An evolutionary role for HIV latency in enhancing viral transmission. Cell *160*, 1002–1012.

Schneider, C.A., Rasband, W.S., and Eliceiri, K.W. (2012). NIH Image to ImageJ: 25 years of image analysis. Nat. Methods *9*, 671–675.

Schwartz, C.J., Giel, J.L., Patschkowski, T., Luther, C., Ruzicka, F.J., Beinert, H., and Kiley, P.J. (2001). IscR, an Fe-S cluster-containing transcription factor, represses expression of Escherichia coli genes encoding Fe-S cluster assembly proteins. Proc. Natl. Acad. Sci. USA *98*, 14895–14900.

Shaner, N.C., Steinbach, P.A., and Tsien, R.Y. (2005). A guide to choosing fluorescent proteins. Nat. Methods *2*, 905–909.

Simon, G., Méjean, V., Jourlin, C., Chippaux, M., and Pascal, M.C. (1994). The torR gene of Escherichia coli encodes a response regulator protein involved in the expression of the trimethylamine N-oxide reductase genes. J. Bacteriol. *176*, 5601–5606.

Sliusarenko, O., Heinritz, J., Emonet, T., and Jacobs-Wagner, C. (2011). High-throughput, subpixel precision analysis of bacterial morphogenesis and intracellular spatio-temporal dynamics. Mol. Microbiol. *80*, 612–627.

Smits, W.K., Kuipers, O.P., and Veening, J.W. (2006). Phenotypic variation in bacteria: the role of feedback regulation. Nat. Rev. Microbiol. *4*, 259–271.

Stella, C., Beckwith-Hall, B., Cloarec, O., Holmes, E., Lindon, J.C., Powell, J., van der Ouderaa, F., Bingham, S., Cross, A.J., and Nicholson, J.K. (2006). Susceptibility of human metabolic phenotypes to dietary modulation. J. Proteome Res. *5*, 2780–2788.

Stewart, M.K., and Cookson, B.T. (2012). Non-genetic diversity shapes infectious capacity and host resistance. Trends Microbiol. *20*, 461–466.

Stubbs, J.R., House, J.A., Ocque, A.J., Zhang, S., Johnson, C., Kimber, C., Schmidt, K., Gupta, A., Wetmore, J.B., Nolin, T.D., et al. (2016). Serum trimethylamine-N-oxide is elevated in CKD and correlates with coronary atherosclerosis burden. J. Am. Soc. Nephrol. *27*, 305–313.

Sureka, K., Ghosh, B., Dasgupta, A., Basu, J., Kundu, M., and Bose, I. (2008). Positive feedback and noise activate the stringent response regulator rel in mycobacteria. PLoS ONE *3*, e1771.

Taniguchi, Y., Choi, P.J., Li, G.W., Chen, H., Babu, M., Hearn, J., Emili, A., and Xie, X.S. (2010). Quantifying E. coli proteome and transcriptome with single-molecule sensitivity in single cells. Science *329*, 533–538.

Tenaillon, O., Skurnik, D., Picard, B., and Denamur, E. (2010). The population genetics of commensal Escherichia coli. Nat. Rev. Microbiol. *8*, 207–217.

Thattai, M., and van Oudenaarden, A. (2004). Stochastic gene expression in fluctuating environments. Genetics *167*, 523–530.

Unden, G., and Bongaerts, J. (1997). Alternative respiratory pathways of Escherichia coli: energetics and transcriptional regulation in response to electron acceptors. Biochim. Biophys. Acta *1320*, 217–234.

Veening, J.W., Smits, W.K., and Kuipers, O.P. (2008a). Bistability, epigenetics, and bet-hedging in bacteria. Annu. Rev. Microbiol. *62*, 193–210.

Veening, J.W., Stewart, E.J., Berngruber, T.W., Taddei, F., Kuipers, O.P., and Hamoen, L.W. (2008b). Bet-hedging and epigenetic inheritance in bacterial cell development. Proc. Natl. Acad. Sci. USA *105*, 4393–4398.

Verstraeten, N., Knapen, W.J., Kint, C.I., Liebens, V., Van den Bergh, B., Dewachter, L., Michiels, J.E., Fu, Q., David, C.C., Fierro, A.C., et al. (2015). Obg and membrane depolarization are part of a microbial bet-hedging strategy that leads to antibiotic tolerance. Mol. Cell *59*, 9–21.

Vinella, D., Loiseau, L., Ollagnier de Choudens, S., Fontecave, M., and Barras, F. (2013). In vivo [Fe-S] cluster acquisition by IscR and NsrR, two stress regulators in Escherichia coli. Mol. Microbiol. *87*, 493–508.

Wadhams, G.H., and Armitage, J.P. (2004). Making sense of it all: bacterial chemotaxis. Nat. Rev. Mol. Cell Biol. *5*, 1024–1037.

Wakamoto, Y., Dhar, N., Chait, R., Schneider, K., Signorino-Gelo, F., Leibler, S., and McKinney, J.D. (2013). Dynamic persistence of antibiotic-stressed mycobacteria. Science *339*, 91–95.

Wang, Z., Tang, W.H., Buffa, J.A., Fu, X., Britt, E.B., Koeth, R.A., Levison, B.S., Fan, Y., Wu, Y., and Hazen, S.L. (2014). Prognostic value of choline and betaine depends on intestinal microbiota-generated metabolite trimethylamine-N-oxide. Eur. Heart J. *35*, 904–910.

Waterhouse, A.M., Procter, J.B., Martin, D.M., Clamp, M., and Barton, G.J. (2009). Jalview Version 2–a multiple sequence alignment editor and analysis workbench. Bioinformatics *25*, 1189–1191.

Waters, C.M., and Bassler, B.L. (2005). Quorum sensing: cell-to-cell communication in bacteria. Annu. Rev. Cell Dev. Biol. *21*, 319–346.

Winter, S.E., Lopez, C.A., and Bäumler, A.J. (2013a). The dynamics of gut-associated microbial communities during inflammation. EMBO Rep. *14*, 319–327.

Winter, S.E., Winter, M.G., Xavier, M.N., Thiennimitr, P., Poon, V., Keestra, A.M., Laughlin, R.C., Gomez, G., Wu, J., Lawhon, S.D., et al. (2013b). Host-derived nitrate boosts growth of E. coli in the inflamed gut. Science *339*, 708–711.

Witte, K., Schuh, A.L., Hegermann, J., Sarkeshik, A., Mayers, J.R., Schwarze, K., Yates, J.R., 3rd, Eimer, S., and Audhya, A. (2011). TFG-1 function in protein secretion and oncogenesis. Nat. Cell Biol. *13*, 550–558.

Zhang, A.Q., Mitchell, S.C., and Smith, R.L. (1999). Dietary precursors of trimethylamine in man: a pilot study. Food Chem. Toxicol. *37*, 515–520.

STAR★METHODS

KEY RESOURCES TABLE

REAGENT or RESOURCE	SOURCE	IDENTIFIER
Chemicals, Peptides, and Recombinant Proteins		
Trimethylamine *N*-oxide dihydrate (TMAO)	Sigma-Aldrich	Cat#T0514; CAS: 62637-93-8
Agarose LE	Dot Scientific	Cat#AGLE
Agarose (Low-Melting)	Fisher BioReagents	Cat#BP165
SeaKem GTG Agarose	Lonza Rockland	Cat#50070
Super Fast Epoxy Cement	Elmer's	Cat#E1009
Experimental Models: Organisms/Strains		
E. coli strain K-12 substrain MG1655	Coli Genetic Stock Center	CGSC#7740
E. coli: JNC73: MG1655 *torS-yfp*-FRT	This paper	N/A
E. coli: JNC74: MG1655 *torS-yfp*-FRT Δ*iscR*::FRT-*kan*-FRT	This paper	N/A
E. coli: JNC92: MG1655 *torT-mcherry*-FRT-*kan*-FRT Δ*torR*	This paper	N/A
E. coli: JNC100: MG1655 *torS-yfp*-FRT-*cat*-FRT *torT-mcherry*-FRT-*kan*-FRT Δ*torR*	This paper	N/A
E. coli: JNC104: MG1655 *torS-yfp*-FRT-*cat*-FRT *torT-mcherry*-FRT-*kan*-FRT Δ*torR* Δ*iscR*::FRT	This paper	N/A
E. coli: JNC112: MG1655 *torS-yfp*-FRT b_{IscR}*	This paper	N/A
E. coli: JNC115: MG1655 b_{IscR}* *torT-mcherry*-FRT-*kan*-FRT Δ*torR*	This paper	N/A
E. coli: JNC116: MG1655 Δ*lacIZY*::P_{torCAD}-*cfp*-FRT-*kan*-FRT *torS-yfp*-FRT b_{IscR}*	This paper	N/A
E. coli: JNC117: MG1655 Δ*lacIZY*::P_{torCAD}-*cfp*-FRT-*kan*-FRT *torS-yfp*-FRT	This paper	N/A
E. coli: JNC122: MG1655 b_{IscR}*	This paper	N/A
E. coli: JNC123: MG1655 attλ::(*cat* P_{torCAD}-*yfp*) b_{IscR}*	This paper	N/A
E. coli: JNC124: MG1655 attλ::(*cat* P_{torCAD}-*yfp*) *torT-cfp*-FRT-*kan*-FRT	This paper	N/A
E. coli: JNC148: MG1655 *torT-mcherry*-FRT Δ*torR*	This paper	N/A
E. coli: JNC157: MG1655 b_{IscR}* *torT-mcherry*-FRT Δ*torR*	This paper	N/A
E. coli: JNC158: MG1655 *torS-yfp*-FRT b_{IscR}* Δ*iscR*::FRT-*kan*-FRT	This paper	N/A
E. coli: JNC159: MG1655 b_{IscR}* *torT-mcherry*-FRT Δ*torR* Δ*iscR*::FRT-*kan*-FRT	This paper	N/A
E. coli: JNC162: MG1655 *torT-mcherry*-FRT Δ*torR* Δ*iscR*::FRT-*kan*-FRT	This paper	N/A
E. coli: JNC163: MG1655 Δ*lacZYA*::FRT-*cat*-FRT *torT-lacZ*-FRT-*kan*-FRT Δ*torR*	This paper	N/A
E. coli: JNC166: MG1655 Δ*lacZYA*::FRT *torS-lacZ*-FRT-*kan*-FRT	This paper	N/A
E. coli: MMR8: MG1655 attλ::(*cat* P_{torCAD}-*yfp*) *ompA-cfp*	Roggiani and Goulian, 2015	N/A
E. coli: MMR14: MG1655 *ompA-cfp* Δ*torC*::FRT	This paper	N/A
E. coli: MMR15: MG1655 attλ::(*cat* P_{torCAD}-*yfp*) *ompA-cfp* Δ*torC*::FRT	This paper	N/A
E. coli: MMR65: MG1655 attλ::(*cat* P_{torCAD}-*yfp*) Δ*xylAFG*::P_{tetA}-*mcherry*-FRT	This paper	N/A
E. coli: PK4854: MG1655 Δ*iscR*::FRT	Schwartz et al., 2001	N/A
Complete list of strains, see Table S1	This paper	N/A

(*Continued on next page*)

Continued

REAGENT or RESOURCE	SOURCE	IDENTIFIER
Oligonucleotides		
Texas Red-b_{IscR}: [T.R.]ATAAAGCCTTATTATTGATGAG GCTATCAT	IDT	N/A
b_{IscR} unlabeled competitor: ATAAAGCCTTATTATTGAT GAGGCTATCAT	IDT	N/A
b_{IscR}* unlabeled competitor: ATAAAGCGTTATTATTGAT GAGGCTATCAT	IDT	N/A
P_{hyaA} unlabeled competitor: ATAAATCCACACAGTTTGT ATTGTTTTGTG	IDT	N/A
Shuffled unlabeled competitor: ATCATCCGTCTTATGTT AATTATAATGGTG	IDT	N/A
PCR primers, see Table S3	This paper	N/A
Software and Algorithms		
IPLab v4.04	BD Biosciences	N/A
NCBI BLAST	Boratyn et al., 2013	https://blast.ncbi.nlm.nih.gov/Blast.cgi
T-Coffee	Notredame et al., 2000	http://tcoffee.crg.cat/apps/tcoffee/index.html
Jalview v2.10.1	Waterhouse et al., 2009	http://www.jalview.org
NimbleScan v2.5	NimbleGen Systems	N/A
Python v2.7.13	Python Software Foundation	https://www.python.org
Python simulation of P_{torCAD}-*yfp* expression	This paper	https://github.com/GoulianLab/tor-simulation
MicrobeJ v5.11y	Ducret et al., 2016	http://www.microbej.com
ImageJ v1.51r	Schneider et al., 2012	https://imagej.nih.gov/ij/
MicrobeTracker v0.937	Sliusarenko et al., 2011	http://microbetracker.org
MATLAB R2012a	MathWorks	N/A

CONTACT FOR REAGENT AND RESOURCE SHARING

Further information and requests for resources and reagents should be directed to and will be fulfilled by the Lead Contact, Mark Goulian (goulian@sas.upenn.edu).

EXPERIMENTAL MODEL AND SUBJECT DETAILS

Bacterial growth media and conditions

All bacterial strains were derived from *Escherichia coli* strain K-12 substrain MG1655. Routine liquid culture was performed in 2 mL LB (Miller) medium at 37°C with aeration on a roller drum, and growth on solid media was performed on LB agar plates at 37°C. When used, antibiotics were added to media at the following concentrations unless otherwise indicated: ampicillin, 100 μg/mL; kanamycin, 25 μg/mL; chloramphenicol 20 μg/mL; and streptomycin, 250 μg/mL.

Liquid cultures for fluorescence microscopy and β-galactosidase assays were grown in 2 mL minimal A medium (Miller, 1992) with 0.2% glucose. For aerobic-to-anaerobic transition microscopy experiments, minimal A medium or M9 medium with 0.2% glycerol was used. M9 medium was supplemented with 0.5 mg/L $FeSO_4 \cdot 7H_2O$. All media contained TMAO at a final concentration of 10 mM except where indicated. For the experiments that produced the data shown in Figure 5, Movie S1, and Figure S6, minimal A medium was also supplemented with 0.1% casamino acids. Cultures were grown with aeration on a roller drum unless otherwise specified. For anaerobic culture, screw-cap culture tubes were filled completely with culture media, inoculated, and sealed tightly with no gas headspace prior to standing incubation at 37°C.

Liquid cultures for ChIP-seq and transcriptomic analysis were grown without TMAO in MOPS minimal medium supplemented with 0.2% glucose (Neidhardt et al., 1974) at 37°C and sparged with a gas mix of 95% N_2 and 5% CO_2 (anaerobic) or 70% N_2, 5% CO_2, and 25% O_2 (aerobic).

METHOD DETAILS

Strain construction

Strains, plasmids, and primers used in this study are listed in Table S1, Table S2, and Table S3, respectively. Transductions were performed with P1*vir* as described previously (Miller, 1992). To make the *torS-yfp* construct, the *yfp* gene with its own ribosome binding site and a linked kanamycin resistance gene with flanking FRT sites was amplified by PCR from template pEB45 using primers torS-yfp-u2 and torS-yfp-l2. The PCR product was recombined into the MG1655 chromosome by recombineering using pKD46 (Datsenko and Wanner, 2000) and correct integration was verified by sequencing. The *torS-yfp* construct was transduced into a clean MG1655 background to create strain MMR149. To make the *torT-mcherry* construct, the *mcherry* gene with its own ribosome binding site and a linked kanamycin resistance gene with flanking FRT sites was amplified by PCR from template pMR5 using primers torT-mcherry-lred-u-v2 and torT-cfp-DtorR-lred-d-v2. The PCR product was recombined into the MG1655 chromosome by recombineering using pKD46 and correct integration was verified by sequencing. The *torT-mcherry* construct was transduced into a clean MG1655 background to create strain JNC92. A *torT-cfp* construct was also made by recombineering: the *cfp* gene with its own ribosome binding site and a linked kanamycin resistance gene with flanking FRT sites was amplified by PCR from template pEB47 using primers torT-cfp-lred-u-v2 and torT-cfp-lred-d-v2. The PCR product was recombined into the MG1655 chromosome using pKD46 and correct integration was verified by sequencing. The *torT-cfp* construct was transduced into a clean MG1655 background to create strain JNC105.

To construct the *torS-yfp torT-mcherry* dual reporter strain JNC100, the kanamycin resistance gene (*kan*) linked to *torS-yfp* in MMR149 was first excised by FLP recombinase using plasmid pCP20 (Cherepanov and Wackernagel, 1995) and then cured of pCP20 to create JNC73 following previously described protocols (Datsenko and Wanner, 2000). JNC73 was then transformed with a different FLP recombinase-expressing plasmid, pEL8, that lacks the *cat* gene. A FRT-*cat*-FRT-containing DNA fragment was amplified by PCR from pKD3 using primers psyn-u1 and oriR6kseqprim1 and introduced into JNC73/pEL8 by electroporation. Cells were allowed to recover with aeration at 37°C for 2.5 h before spreading a portion on LB plates with 6 μg/mL chloramphenicol. Colonies were purified on LB plates with 20 μg/mL chloramphenicol to create JNC99. JNC99 was tested for loss of pEL8 by confirmation of ampicillin sensitivity and for proper integration of the *cat* gene by PCR. The *torT-mcherry* construct was transduced from JNC92 into JNC99 with selection on plates containing kanamycin and chloramphenicol to ensure maintenance of the *torS-yfp* fusion.

The Keio collection of single-gene knockouts (Baba et al., 2006) was used for construction of Δ*iscR* and Δ*torC* strains. The Δ*iscR* construct was moved by transduction from JW2515 into JNC73 to create JNC74, into JNC148 (see below) to create JNC162, and into MG1655 to create MMR213. The kanamycin resistance gene of MMR213 was excised using pCP20, and the strain was cured of pCP20 to create JNC102. The *torS-yfp* and *torT-mcherry* fusions were moved into JNC102 by transduction from JNC100 to create JNC104. The Δ*iscR* construct from JW2515 was moved into the P_{torCAD}-*yfp ompA-cfp* strain MMR8 (Roggiani and Goulian, 2015) by transduction to create MMR210. The Δ*torC* construct was moved by transduction from JW0981 into EPB47 to create MMR11 and into MMR8 to create MMR12. The kanamycin resistance gene of MMR11 was excised using pCP20 and the strain cured of pCP20 to create MMR14. The same method was used to remove the kanamycin resistance gene from MMR12, creating MMR15.

The *torT-lacZ* reporter strain JNC163 was constructed by deleting *lacZYA* in JNC92 and replacing the *mcherry* gene with *lacZ* by recombineering. The kanamycin resistance gene of JNC92 was excised using pCP20 to create JNC148, and the *lacZYA* deletion was introduced from strain TIM89 by transduction to create JNC161. The *lacZ* construct for the *torT-lacZ* reporter was generated by overlap extension PCR: the first DNA segment was amplified from MG1655 genomic DNA using primers torT-lacZ-lred-u and lacZcterm-l1, and the second DNA segment was amplified from the Keio Δ*lacY* strain JW0334 using primers lacY-Keio-u and torT-lacZ-lred-l. The assembled *lacZ-kan* construct was integrated downstream of *torT* in JNC161 by pKD46-mediated recombination, and correct integration was verified by sequencing. The construct was transduced into a clean JNC161 background to create strain JNC163. The *torS-lacZ* reporter strain JNC166 was constructed by amplifying *lacZ-kan* from JNC163 using primers torS-lacZ-lred-u2 and torS-lacZ-lred-l2 and integrating it downstream of *torS* in the Δ*lacZYA* strain TIM183 by pKD46-mediated recombination. Correct integration was verified by PCR.

The P_{torCAD}-*yfp* transcriptional reporter integrated into the chromosome of MG1655 at the phage λ attachment site in strains MMR7 and MMR8 is described in (Roggiani and Goulian, 2015), as is the P_{tetA}-*mcherry* fusion incorporated at the *xyl* locus in strain MMR59. The P_{tetA}-*mcherry* fusion was moved from MMR59 into MMR7 by transduction to create MMR64, and the kanamycin resistance gene marking P_{tetA}-*mcherry* was eliminated by pCP20-mediated FLP recombination to create MMR65. JNC124, a strain containing the P_{torCAD}-*yfp* transcriptional reporter and the *torT-cfp* operon fusion, was constructed by transduction using MMR7 as the donor strain and JNC105 as the recipient strain.

Point mutations in the IscR binding site between *torS* and *torT* were constructed using a scarless mutagenesis technique (Blank et al., 2011). The point mutation is a C-to-G substitution at the −21 position relative to the *torT* transcription start site (a sequence change from 5′-AAAGC**C**TTATT-3′ to 5′-AAAGC**G**TTATT-3′), denoted b_{IscR}*. To introduce b_{IscR}* into a *torS-yfp* reporter strain, a DNA fragment containing an I-SceI cut site and chloramphenicol resistance gene was amplified from pWRG100 using primers PtorT-PtorS-pWRG100 and torT-pWRG100 and integrated at the *tor* locus of JNC73 by recombineering using pKD46. Correct integration was confirmed by PCR, and the strain was cured of pKD46 to create JNC109. JNC109 was transformed with pWRG99, a derivative of pKD46 that contains a tetracycline-inducible I-SceI gene, and a DNA fragment containing the b_{IscR}* mutation and homology to the chromosomal sequencing flanking the I-SceI cut site was incorporated into the chromosome. DNA incorporation was

achieved by plating on 0.5 μg/mL anhydrotetracycline to induce expression of I-SceI so as to inhibit growth of cells containing a chromosomal I-SceI cut site (i.e., cells that failed to replace the I-SceI cut site with the introduced DNA harboring the b_{IscR}* mutation). The resulting strain was JNC112. The DNA fragment containing b_{IscR}* was generated by overlap extension PCR using MG1655 genomic DNA as a template with outer primers HK022-P1 and HK022-P4 and inner primers iscRbs-mut2-mid-r and iscRbs-mut2-mid-f. The chromosomal b_{IscR}* mutation was verified by sequencing, and JNC112 was confirmed to be ampicillin and chloramphenicol sensitive. The Δ*iscR* mutation was moved from JW2515 into JNC112 by transduction to create JNC158.

JNC115, the *torT-mcherry* reporter strain harboring the b_{IscR}* mutation, was constructed in a manner analogous to that of JNC112. The I-SceI cut site construct was first introduced into MG1655 by recombineering to create JNC108 and then transduced from JNC108 into JNC92 using P1*vir* to create JNC111. JNC111 was transformed with pWRG99, and b_{IscR}* was incorporated by electroporation of DNA with flanking homology and counterselection against I-SceI cut site-containing cells. JNC115 was verified by sequencing and confirmed to be ampicillin and chloramphenicol sensitive. This counterselection procedure was also used directly in JNC108 to create JNC122, which is identical to MG1655 but with the single point mutation b_{IscR}*. All PCR primers and templates were the same as those used in the construction of JNC112. The kanamycin resistance gene of JNC115 was excised using pCP20 to create JNC157. The Δ*iscR* mutation was moved from JW2515 into JNC157 by transduction to create JNC159.

The P_{torCAD}-*cfp* transcriptional reporter was amplified from pMR19 using primers lac-pMR10-U1 and lac-pMR10-L1 and integrated into the chromosome of MG1655 by recombineering to create MMR67. This construct was transduced into JNC73 to create the P_{torCAD}-*cfp torS-yfp* strain JNC117 and into JNC112 to create the P_{torCAD}-*cfp torS-yfp* b_{IscR}* strain JNC116. A different P_{torCAD} reporter strain with the b_{IscR}* mutation, JNC123, was constructed by transduction of P_{torCAD}-*yfp* from MMR7 into JNC122.

Phase contrast and fluorescence microscopy

Liquid cultures in minimal medium without TMAO were inoculated from single colonies on LB agar plates and grown to saturation overnight. Cultures were diluted 1:1000 or 1:500 into fresh medium with TMAO and grown aerobically or anaerobically (as described above) to an optical density at 600 nm of 0.1 to 0.2. Cultures were then placed on ice and streptomycin was added to halt further protein synthesis. For experiments involving comparisons of aerobic and anaerobic growth of bacteria expressing fluorescent proteins, all of the cultures were aerated on a roller drum after streptomycin addition to allow for fluorophore maturation before imaging. For experiments employing mCherry and/or YFP, aeration occurred at room temperature overnight. For experiments employing both CFP and YFP, cultures were held at 4°C overnight and then aerated at 4°C or room temperature for 2 – 3 h. For experiments involving only aerobic growth, cultures were held at 4°C overnight after streptomycin addition. Cultures were kept on ice until time of imaging. Cells were immobilized for imaging by placing 5 μL culture on a 75 μL 1% agarose LE pad prepared in minimal A salts as described in Miyashiro and Goulian (2007). Imaging was performed on an Olympus IX81 inverted microscope equipped with a 100 W mercury lamp and a UPlanApo 100 × NA 1.35 oil immersion objective and filter sets from Chroma. Excitation filters, dichroic mirrors, and emission filters for CFP, YFP, and mCherry were D436/20x, 455dclp, D480/40 m; HQ500/20x, Q515lp, HQ535/30 m; and HQ575/50x, Q610lp, HQ640/50 m, respectively. Images were acquired with a SensiCam QE CCD camera operated at −12°C or an Andor iXon EMCCD operated at −20°C. Electron-multiplying gain was employed when imaging strains containing the *torS-yfp* or *torT-mcherry* reporter constructs. IPLab v3.7 software was used to record images.

Aerobic-to-anaerobic transition microscopy

Single colonies of fluorescent reporter strains and a non-fluorescent oxygen-scavenging strain (MG1655) were used to inoculate liquid cultures in minimal A medium plus glycerol without TMAO. Cultures were grown to saturation overnight and then diluted 1:100 (fluorescent reporter strains) or 1:50 (oxygen-scavenging strain) into M9 glycerol medium plus TMAO and ferrous sulfate and grown with aeration for 5 h. After 5 h, an agarose pad containing embedded oxygen-scavenging cells was prepared as follows. 3% Low-melting agarose in M9 salts plus ferrous sulfate was boiled and then cooled to 42°C. A 1:1 mixture of MG1655 from the saturated overnight culture and MG1655 from the growing culture was prepared, and this cell mixture was then mixed with the molten low-melt agarose in a 1:1 ratio (making the final agarose concentration 1.5%). Glycerol and TMAO were added to the cell/agarose mixture to final concentrations of 0.2% and 10 mM, respectively. The cell-embedded agarose pad was cast by depositing 1 mL of the agarose/cells mixture on a 22 × 22 mm cover glass and floating another 22 × 22 mm cover glass on top. The pad was allowed to solidify for 45 min, and then one cover glass was removed and the pad transferred to a standard microscope slide (so that the pad is sandwiched between slide and cover glass) with care taken to avoid trapping air bubbles between the slide and the agarose pad.

To inoculate the agarose pad, the cover glass was removed and 5 μL fluorescent reporter strain culture was deposited on the pad surface. This 5 μL contained a 1:1 mixture of P_{torCAD}-*yfp* reporter strain and, as a control for anaerobiosis, a CFP-fluorescent strain unable to grow anaerobically in M9 glycerol medium plus TMAO (strain MMR14). A smaller (18 × 18 mm) cover glass was applied to the inoculated pad with care taken to avoid air bubbles. Any trapped air bubbles were removed by sliding the cover glass along the pad surface until the bubbles were liberated and then sliding the cover glass back to the center of the pad. The edges of the agarose pad were trimmed with a razor blade to reduce the pad area to that of the 18 × 18 mm cover glass. The entire pad perimeter between cover glass and slide was then sealed with epoxy cement, which was allowed to set for 5 min. The prepared slide was moved to a

microscope stage in a temperature-controlled chamber set to 34°C for time lapse imaging. Images were taken immediately after positioning the slide on the stage and within 30 minutes of sealing with epoxy, and this time was designated the start time (t = 0 min) of anaerobiosis.

The control strain for anaerobiosis, MMR14, is Δ*torC* and constitutively expresses CFP to allow its identification during microscopy. Because the growth medium contains only a non-fermentable carbon source (glycerol) and no respiratory electron acceptors other than TMAO, a Δ*torC* strain cannot grow within the time frame analyzed unless the system is contaminated with sufficient oxygen for aerobic respiration. During each experiment, at least 50 randomly selected P_{torCAD}-*yfp* cells and at least 50 randomly selected Δ*torC* cells were monitored for growth, and lack of growth was confirmed for Δ*torC* cells (Figures S1B and S1C).

For the experiment shown in Figure S1D (mock aerobic-to-anaerobic transition), fluorescent reporter strains were grown exactly as described above. The agarose pad was prepared as above but without the embedded oxygen-scavenging cells. Bacterial culture (5 μL) was deposited into the center of a cover-glass bottom cell culture dish (FluoroDish; World Precision Instruments Cat#FD35-100), and the agarose pad was placed on top of the culture. The inner perimeter of the dish was lined with a Kimwipe moistened with M9 salts plus ferrous sulfate to maintain hydration of the agarose pad during the course of the experiment. The lid of the dish was treated with anti-fogging agent (Cat Crap; EK Cat#10003B), sealed with plastic paraffin film, and transferred to a microscope stage in a temperature-controlled chamber for imaging. The chamber was maintained at 34°C for the duration of the experiment.

Time-lapse microscopy

To produce Movie S1, time-lapse microscopy of aerobically growing microcolonies was performed as previously described (Roggiani and Goulian, 2015) with slight modifications. Liquid cultures in minimal A medium plus casamino acids and glucose without TMAO were inoculated from single colonies on LB agar plates and grown to saturation overnight. Cultures were diluted 1:1000 into minimal A medium plus casamino acids, glucose, and TMAO and grown for 3.5 h. An agarose pad was prepared by dissolving 1% SeaKem GTG agarose in minimal A salts. When the agarose solution reached a temperature of 55°C, $MgSO_4$ (1 mM final), glucose (0.2% final), casamino acids (0.1% final), and TMAO (10 mM final) were added. The agarose solution was poured into a cover-glass bottom cell culture dish to a depth of approximately 5 mm and allowed to solidify. After solidification, the agarose pad was warmed to 37°C and inoculated by lifting the pad with a spatula, depositing 5 μL bacterial culture into the center of the dish, and lowering the pad. The lid of the dish was treated with an anti-fogging agent, sealed, and transferred to a microscope stage in a temperature-controlled chamber as described above. The chamber was maintained at 32°C for the duration of the experiment, and phase-contrast and fluorescence images were collected every 14 min.

β-Galactosidase assays

Liquid cultures in minimal medium without TMAO were inoculated from single colonies on LB agar plates and grown to saturation overnight. Cultures were diluted 1:1000 into fresh medium with TMAO and grown aerobically or anaerobically as described above. Cells were harvested at an optical density at 600 nm of 0.1 to 0.2, and the assay performed as in Miller (1992).

Sequence alignment

Bacterial genomes containing DNA sequence similar to that of the *E. coli torS* and *torT* genes were identified using NCBI BLAST (Boratyn et al., 2013). Alignment of the intergenic DNA sequences was performed using T-Coffee (Notredame et al., 2000), and visualization of the alignment was produced using Jalview (Waterhouse et al., 2009).

ChIP-seq and transcriptomics

Strains MG1655 (wild-type) and PK4854 (Δ*iscR*) were grown in MOPS minimal medium without TMAO aerobically and anaerobically as described above. Cells were harvested for processing during mid-exponential phase ($OD_{600} \cong 0.3$). ChIP-seq analysis for IscR was performed as previously described (Myers et al., 2013). The IscR antibody was affinity purified as described previously (Witte et al., 2011). ChIP-seq data for σ^{70} was obtained from Myers et al. (2013).

Total RNA was isolated as previously described (Khodursky et al., 2003). The concentration of the purified RNA was determined using a NanoDrop 2100, while the integrity of the RNA was analyzed using gel electrophoresis. The RNA isolated from MG1655 or PK4854 cultures grown under either aerobic or anaerobic conditions was converted into strand specific, single-stranded cDNA as described previously (Cho et al., 2009). The cDNA was labeled with Cy3 and then hybridized to custom designed, high-density tiled microarrays containing 378,000 probes from alternate strands, spaced roughly every 12 bp through the genome as described previously (Cho et al., 2009). Microarray hybridization and scanning were performed as described previously (Myers et al., 2013) and the photomultiplier tube was adjusted until the median background value was approximately 100. All probe data were normalized using Robust Multiarray Average in the NimbleScan software package, version 2.5 (Irizarry et al., 2003). The median of the normalized probe signal within previously identified open reading frames was averaged between two biological replicates.

DNA-binding fluorescence polarization assays

DNA-binding isotherms were generated by measuring changes in fluorescence polarization when IscR-C92A, purified as previously described (Giel et al., 2006; Nesbit et al., 2009), bound a 30 bp dsDNA fragment, one strand of which was linked to a Texas Red

fluorophore at the 5′ end. This fragment contained 25-bp of the predicted type 2 IscR binding site identified within the *torT* promoter region (5′-ATAAAGCCTTATTATTGATGAGGCTATCAT-3′, denoted b_{IscR}) based on similarity to the consensus type 2 motif (5′-AxxxCCxxAxxxxxxxTAxGGxxxT-3′) (Nesbit et al., 2009). To demonstrate the specificity of binding, equilibrium-competition assays were used in which IscR-C92A (120nM) was incubated with the Texas Red-labeled b_{IscR} fragment (5 nM) in the presence of unlabeled competitor DNA (8-1000 nM) in 40 mM Tris (pH 7.9), 150 mM KCl, 5% glycerol, and 10 μM DTT, and fluorescence anisotropy was measured upon addition of varying amounts of non-fluorescent competitor DNA. The non-fluorescent competitor DNA was either: 1) b_{IscR} (i.e., the same sequence as the fluorescently labeled oligonucleotide); 2) b_{IscR}* (a C-to-G substitution at position 8 of b_{IscR}); 3) the IscR binding site sequence from the well-characterized type 2 site in the *hyaA* promoter region (Giel et al., 2006; Nesbit et al., 2012); or 4) shuffled DNA sequence with no resemblance to b_{IscR}. The annealing of complementary DNA strands, fluorescence measurements, fraction bound determination, and data fitting were performed as previously described (Rajagopalan et al., 2013); however, all manipulations were carried out under aerobic conditions. Assays were repeated on three independent occasions.

ChIP-qPCR analysis

ChIP assays for strains MG1655 and JNC122 were performed as previously described (Davis et al., 2011) except that cultures were grown under aerobic conditions in minimal A glucose medium containing 10 mM TMAO. Samples were immunoprecipitated using a polyclonal antibody raised against IscR that had been absorbed against a mutant strain lacking *iscR*. Promoter DNA from ChIP samples was quantified by real-time PCR using SYBR Green JumpStart (Sigma-Aldrich) and a BioRad CFX96 Real-Time PCR Detection System. Primer sequences for amplifying the *torT*, *hyaA*, and *ydfZ* promoters are provided in Table S3 (PtorT-forward and PtorT-reverse; PhyaA-forward and PhyaA-reverse; and PydfZ-forward and PydfZ-reverse).

Computer simulations

The computer simulation of P_{torCAD}-*yfp* expression was implemented in Python. The simulation initializes a parent cell with a random number of TorS and TorT molecules (within the estimated range of the number of molecules produced in a generation, obtained from published values (Li et al., 2014; Taniguchi et al., 2010) and drawn from a Gamma distribution). The parent cell is then permitted to "divide" for ten generations with lineage information preserved. The computer simulation makes use of several simplifying assumptions regarding the behavior of the TorT/TorS/TorR signaling pathway and *torCAD* expression to isolate the key question of interest: whether a modest increase in population-wide distribution of TorT and TorS protein can have a significant effect on the behavior of *torCAD* expression. At each division, the amount of free TorS, free TorT, and TorST complex is computed assuming that every TorS and TorT molecule will form a complex if a partner is available (i.e., there is only free TorS or TorT if one is present in excess of the other). TMAO is assumed to be present in saturating levels so that every TorT in a TorST complex has TMAO bound. Equilibration of the concentration of phosphorylated TorR is assumed to occur instantaneously, and the fraction of phosphorylated TorR is then calculated from the following equation (which includes the implicit assumption that the rate constants for TorR phosphorylation by TorST and TorR-P dephosphorylation by TorS are equal):

$$\frac{TorR-P}{TorR_{tot}}=\frac{TorST}{TorST+TorS_{free}}$$

where $TorR_{tot}$ is the total number of TorR molecules in the cell and is arbitrary for the purposes of this simulation.

In the interval between divisions, the cell synthesizes YFP, TorS, and TorT. The number of YFP molecules produce by the P_{torCAD}-*yfp* reporter is taken to be directly proportional to the amount of TorR-P in the cell. The amounts of TorS and TorT produced are drawn from the Gamma distribution:

$$p(x)=\frac{1}{b^a\Gamma(a)}x^{a-1}e^{-x/b}$$

where *p(x)* is the distribution of a protein in a population of cells, *x* is the concentration of the protein in a cell, *a* is the mean number of protein production bursts per division cycle (assuming no active protein degradation), and *b* is the mean number of proteins produced per burst (Friedman et al., 2006). The product of *a* and *b* is the mean number of protein molecules per cell in the population, which we know to be very low under aerobic conditions. We assume that *b,* the mean number of molecules produced per burst, is unaffected by the presence or absence of oxygen – i.e., that there is no post-transcriptional oxygen-dependent regulation of TorT and TorS production. This assumption allows us to fix the value of *b* for TorT and TorS and explore the effect of varying the value of *a* on downstream P_{torCAD} activity. For simplicity, we set $b = 1$ and only allowed *a* to vary when simulating different levels of repression of *torS* and *torT*. At cell division, the simulation allows TorS, TorT, and TorTS complex to partition randomly between the daughter cells and distributes YFP evenly between the daughters. The lifetime of YFP protein is assumed to be infinite, only decreasing by dilution through cell division.

QUANTIFICATION AND STATISTICAL ANALYSIS

Analysis of fluorescent reporters of gene expression in single cells was performed using the MicrobeJ plugin (Ducret et al., 2016) for ImageJ (Schneider et al., 2012) or the MicrobeTracker Suite for MATLAB (Sliusarenko et al., 2011). Background subtraction of images was performed prior to fluorescence quantification using the ImageJ sliding paraboloid algorithm or by subtraction of the mean background as described in Miyashiro and Goulian (2007). Single-cell fluorescence was quantified as mean fluorescence per cell (total cellular fluorescence divided by cell area), with cell area determined by particle detection and segmentation of the corresponding phase contrast images. The mean fluorescence of each dataset was calculated by averaging the single-cell fluorescence of at least 100 cells. Cellular autofluorescence in each channel was determined by including in each experiment a control strain lacking the fluorescent reporter(s) of interest. The mean autofluorescence was subtracted from the mean fluorescence for each dataset.

Microcolony areas for aerobic-to-anaerobic transition experiments were determined by summing the lengths of all cells in the microcolony and multiplying by a constant cell width. Parent cell areas were calculated using the same method. The limit of detection for cell growth in the aerobic-to-anaerobic transition experiments was determined by calculating the maximum apparent fold change in cell area for approximately 200 non-growing cells over 5 h. Apparent fold changes in cell area result from slight differences in image focus between the start and end of an experiment.

Statistical parameters for each experiment are reported in the relevant figure legends.

DATA AND SOFTWARE AVAILABILITY

The Python source code for the computer simulation of P_{torCAD}-*yfp* expression is publicly available at https://github.com/GoulianLab/tor-simulation.

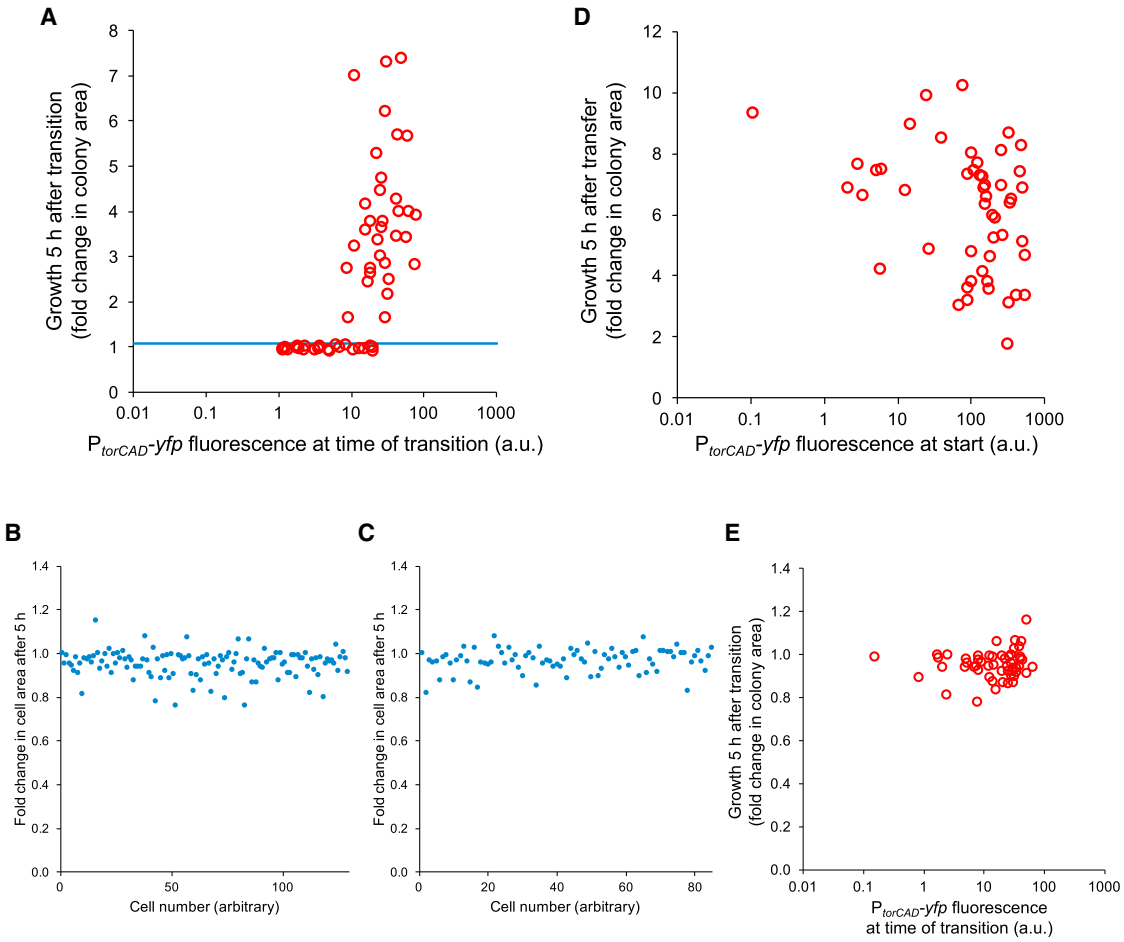

Figure S1. Cell-to-Cell Variability in *torCAD* Expression Permits a Subpopulation to Continue Growth through a Transition to Anaerobiosis, Related to Figure 1

(A) Each circle represents a cell or microcolony of the P_{torCAD}-*yfp* P_{tetA}-*mcherry* strain MMR65. Growth is quantified as the ratio of microcolony area approximately 5 h after O_2 depletion to the area of the parent cell at the time of depletion. The blue line indicates the limit of detection for cell growth. Data are shown from a single experiment in which at least 50 randomly selected cells were monitored for growth. The apparent smaller range of fluorescence values for dark (non-growing) cells in these data compared to the data shown in Figure 1C is due to differences in the background subtraction algorithms used to process the two data sets. For Figure 1C, background was subtracted as described in (Miyashiro and Goulian, 2007). For this figure, the ImageJ sliding paraboloid algorithm was used (Schneider et al., 2012). Fluorescence from the P_{torCAD}-*yfp* reporter is dim in some aerobically growing cells, so different algorithms were used to confirm that results were unaffected by the background subtraction method. a.u., arbitrary units.

(B) For the experiment shown in Figure 1C, the Δ*torC* CFP^+ strain MMR14 was grown in identical culture conditions to those of the P_{torCAD}-*yfp* reporter strain MMR65. The two strains were mixed before inoculating the anaerobic agarose pad for microscopy. Randomly selected Δ*torC* CFP^+ cells were monitored for growth during the experiment to ensure that the agarose pad was free of O_2 contamination. A fold change in cell area of 1.0 indicates no growth. Small changes in focus over the 5 h experiment account for departures from a fold change in area of 1.0.

(C) Same as (B), but for the experiment depicted in (A).

(D) The P_{torCAD}-*yfp* P_{tetA}-*mcherry* strain MMR65 was transferred to an aerobic rather than an anaerobic agarose pad and monitored for growth for 5 h after transfer.

(E) A strain carrying the P_{torCAD}-*yfp* reporter but lacking the *torC* gene (MMR15) was subjected to the same experimental procedure as in (A) and did not grow after the transition to anaerobiosis.

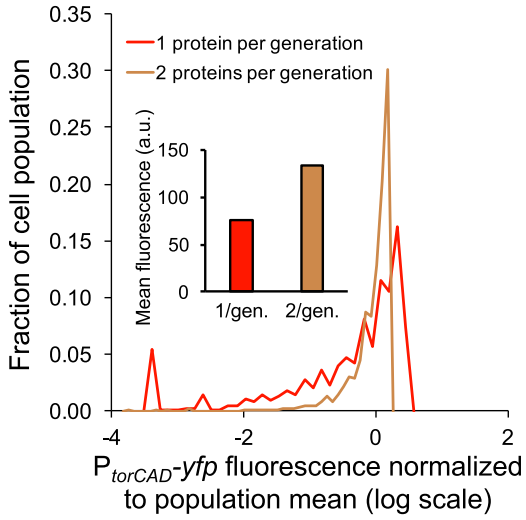

Figure S2. Simulated Distributions of P_{torCAD}-*yfp* Fluorescence for Different Rates of TorT and TorS Protein Production, Related to Figure 2

Distributions were simulated for average protein production rates of one copy per generation (red) and two copies per generation (brown). The plotted distributions represent the cumulative results from 100 independent runs of the simulation for each condition. Inset: Simulated mean P_{torCAD}-*yfp* fluorescence for the displayed distributions.

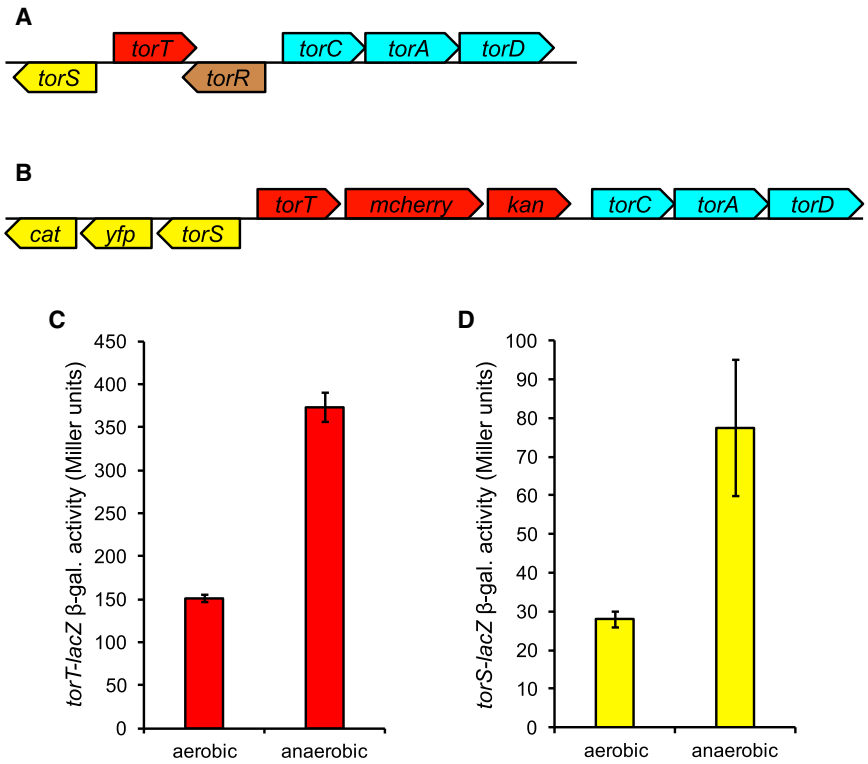

Figure S3. Schematics of *torT* and *torS* Reporter Constructs and Behavior of *lacZ* Transcriptional Fusions, Related to Figure 2

(A) Schematic of the wild-type *E. coli tor* locus.

(B–D) Schematic of the *tor* locus of the *torT-mcherry torS-yfp* transcriptional reporter strain (JNC100). The *torR* gene was deleted from the reporter strain because of its overlap with *torT*. TorR is not involved in the regulation of *torT* or *torS* expression. *kan*, kanamycin resistance gene; *cat*, chloramphenicol resistance gene. Transcriptional fusions of *lacZ* to (C) *torT* (JNC163) and (D) *torS* (JNC166) were used to corroborate the results from the fluorescent protein reporters shown in Figure 2C. Growth conditions were identical between the fluorescent protein and *lacZ* reporter experiments. Bar heights represent the mean values for five independent experiments, and error bars represent standard deviations.

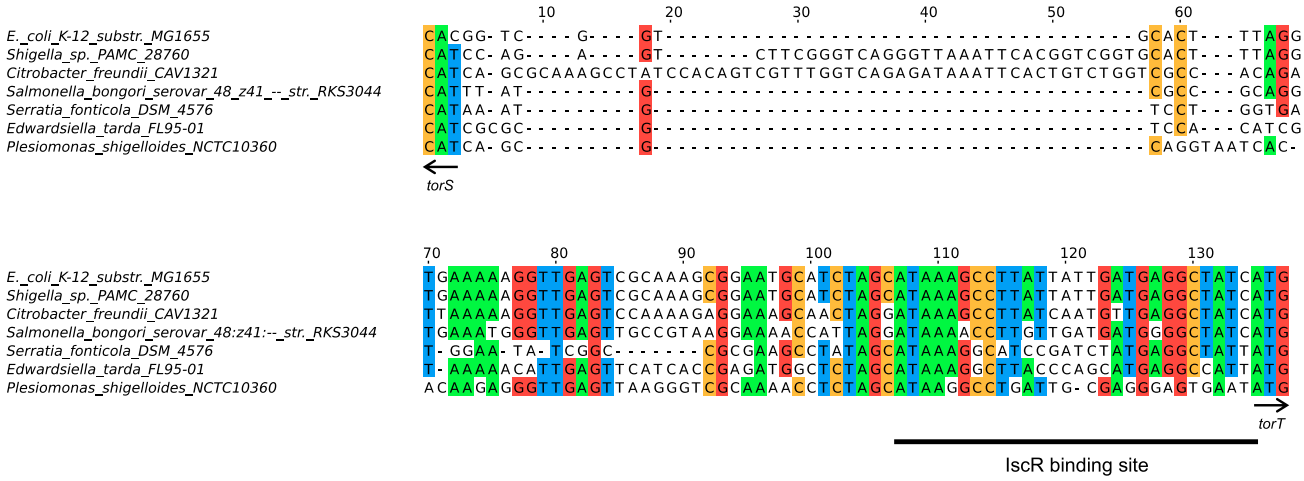

Figure S4. The *torT-torS* Intergenic Region Shows a High Degree of Sequence Conservation across Members of the *Enterobacteriaceae*, Related to Figure 3

Bases with greater than 70% identity conservation are shaded. The degree of conservation in the vicinity of the IscR binding site is particularly high.

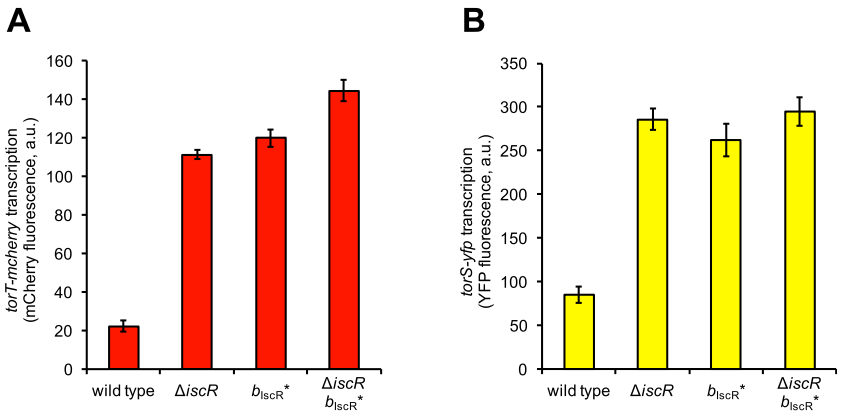

Figure S5. The b_{IscR}* Mutation Has No Significant Effect on *torS* Transcription and a Very Small Effect on *torT* Transcription in a Δ*iscR* Strain, Related to Figure 4

Deletion of *iscR* and/or introducing the b_{IscR}* IscR binding site mutation increases aerobic transcription of *torT* and *torS*.

(A) Fluorescent *torT-mcherry* reporter strains with wild-type *iscR* (JNC148), Δ*iscR* (JNC162), b_{IscR}* (JNC157) or Δ*iscR* b_{IscR}* (JNC159) were grown aerobically in minimal glucose medium with TMAO and analyzed by fluorescence microscopy.

(B) Fluorescent *torS-yfp* reporter strains with wild-type *iscR* (JNC73), Δ*iscR* (JNC74), b_{IscR}* (JNC112) or Δ*iscR* b_{IscR}* (JNC158) were grown and analyzed as in (A).

Bar heights represent the mean values for three independent experiments, and error bars represent standard deviations. a.u., arbitrary units.

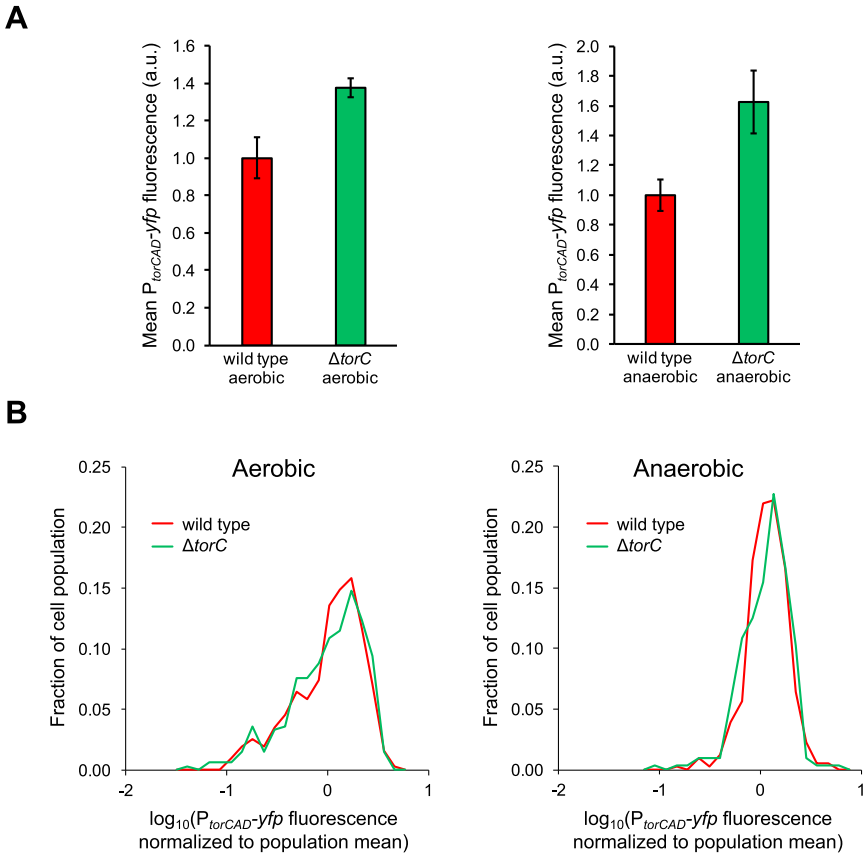

Figure S6. Deletion of *torC* Increases Mean Expression from P$_{torCAD}$ but Does Not Affect Variability, Related to Figure 5

Fluorescent P$_{torCAD}$-*yfp* reporter strains with wild-type *torC* (MMR8) or Δ*torC* (MMR15) were grown aerobically or anaerobically in minimal glucose medium with casamino acids and TMAO and analyzed by fluorescence microscopy. The strains constitutively express cyan fluorescent protein (CFP) for fluorescence normalization (Roggiani and Goulian, 2015).

(A) Mean single-cell fluorescence of wild-type and Δ*torC* strains grown aerobically or anaerobically. Fluorescence for each cell was quantified as YFP fluorescence normalized by the CFP internal standard. Bar heights represent the mean values for two independent experiments, and error bars represent the ranges. a.u., arbitrary units.

(B) Distributions of single-cell fluorescence for wild-type and Δ*torC* strains grown aerobically or anaerobically. Values on the *x*-axis are expressed as fluorescence normalized by the mean value from the corresponding data set. Each data set consists of combined measurements from two independent experiments.

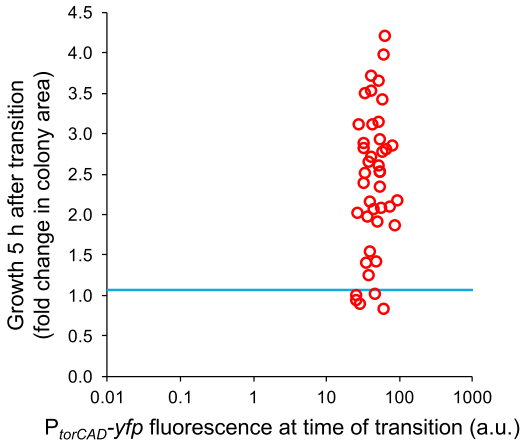

Figure S7. Uniform Expression of *torCAD* Permits Growth of Nearly the Entire Population after O_2 Depletion (Replicate Experiment), Related to Figure 7

Each circle represents a cell or microcolony of the P$_{torCAD}$-*yfp* b_{IscR}* strain JNC123. Growth is quantified as the ratio of microcolony area approximately 5 h after O_2 depletion to the area of the parent cell at the time of depletion. The blue line indicates the limit of detection for cell growth. Data are shown from a single experiment in which at least 50 randomly selected cells were monitored for growth. a.u., arbitrary units.